NASA/CR-2002-211452
ICASE Report No. 2002-4

Influence of 2D Finite Element Modeling Assumptions on Debonding Prediction for Composite Skin-stiffener Specimens Subjected to Tension and Bending

Ronald Krueger
ICASE, Hampton, Virginia

Pierre J. Minguet
The Boeing Company, Philadelphia, Pennsylvania

March 2002

The NASA STI Program Office . . . in Profile

Since its founding, NASA has been dedicated to the advancement of aeronautics and space science. The NASA Scientific and Technical Information (STI) Program Office plays a key part in helping NASA maintain this important role.

The NASA STI Program Office is operated by Langley Research Center, the lead center for NASA's scientific and technical information. The NASA STI Program Office provides access to the NASA STI Database, the largest collection of aeronautical and space science STI in the world. The Program Office is also NASA's institutional mechanism for disseminating the results of its research and development activities. These results are published by NASA in the NASA STI Report Series, which includes the following report types:

- TECHNICAL PUBLICATION. Reports of completed research or a major significant phase of research that present the results of NASA programs and include extensive data or theoretical analysis. Includes compilations of significant scientific and technical data and information deemed to be of continuing reference value. NASA's counterpart of peer-reviewed formal professional papers, but having less stringent limitations on manuscript length and extent of graphic presentations.

- TECHNICAL MEMORANDUM. Scientific and technical findings that are preliminary or of specialized interest, e.g., quick release reports, working papers, and bibliographies that contain minimal annotation. Does not contain extensive analysis.

- CONTRACTOR REPORT. Scientific and technical findings by NASA-sponsored contractors and grantees.

- CONFERENCE PUBLICATIONS. Collected papers from scientific and technical conferences, symposia, seminars, or other meetings sponsored or cosponsored by NASA.

- SPECIAL PUBLICATION. Scientific, technical, or historical information from NASA programs, projects, and missions, often concerned with subjects having substantial public interest.

- TECHNICAL TRANSLATION. English-language translations of foreign scientific and technical material pertinent to NASA's mission.

Specialized services that complement the STI Program Office's diverse offerings include creating custom thesauri, building customized data bases, organizing and publishing research results . . . even providing videos.

For more information about the NASA STI Program Office, see the following:

- Access the NASA STI Program Home Page at ***http://www.sti.nasa.gov***

- Email your question via the Internet to help@sti.nasa.gov

- Fax your question to the NASA STI Help Desk at (301) 621-0134

- Telephone the NASA STI Help Desk at (301) 621-0390

- Write to:
  NASA STI Help Desk
  NASA Center for AeroSpace Information
  7121 Standard Drive
  Hanover, MD 21076-1320

NASA/CR-2002-211452
ICASE Report No. 2002-4

Influence of 2D Finite Element Modeling Assumptions on Debonding Prediction for Composite Skin-stiffener Specimens Subjected to Tension and Bending

Ronald Krueger
ICASE, Hampton, Virginia

Pierre J. Minguet
The Boeing Company, Philadelphia, Pennsylvania

ICASE
NASA Langley Research Center
Hampton, Virginia

Operated by Universities Space Research Association

Prepared for Langley Research Center
under Contract NAS1-97046

March 2002

Available from the following:

NASA Center for AeroSpace Information (CASI)
7121 Standard Drive
Hanover, MD 21076-1320
(301) 621-0390

National Technical Information Service (NTIS)
5285 Port Royal Road
Springfield, VA 22161-2171
(703) 487-4650

INFLUENCE OF 2D FINITE ELEMENT MODELING ASSUMPTIONS ON DEBONDING PREDICTION FOR COMPOSITE SKIN-STIFFENER SPECIMENS SUBJECTED TO TENSION AND BENDING

RONALD KRUEGER* AND PIERRE J. MINGUET+

Abstract. The influence of two-dimensional finite element modeling assumptions on the debonding prediction for skin-stiffener specimens was investigated. Geometrically nonlinear finite element analyses using two-dimensional plane-stress and plane-strain elements as well as three different generalized plane strain type approaches were performed. The computed deflections, skin and flange strains, transverse tensile stresses and energy release rates were compared to results obtained from three-dimensional simulations. The study showed that for strains and energy release rate computations the generalized plane strain assumptions yielded results closest to the full three-dimensional analysis. For computed transverse tensile stresses the plane stress assumption gave the best agreement. Based on this study it is recommended that results from plane stress and plane strain models be used as upper and lower bounds. The results from generalized plane strain models fall between the results obtained from plane stress and plane strain models. Two-dimensional models may also be used to qualitatively evaluate the stress distribution in a ply and the variation of energy release rates and mixed mode ratios with delamination length. For more accurate predictions, however, a three-dimensional analysis is required.

Key words. composite materials, delamination, finite element analysis, fracture mechanics

Subject classification. Structures and Materials

1. Background. Many composite components in aerospace structures are made of flat or curved panels with co-cured or adhesively bonded frames and stiffeners. Previous investigations of the failure of secondary bonded structures focused on loading conditions typically experienced by aircraft crown fuselage panels. Tests were conducted with specimens cut from a full-size panel to verify the integrity of the bondline between the skin and the flange or frame [1]. A simpler and cheaper specimen configuration that would allow detailed observations of the failure mechanism at the skin/flange interface was proposed in reference [2]. The investigations focused on the failure mechanisms of a bonded skin/flange coupon configuration subjected to tension, three and four-point bending, and combined tension/bending loading [3-6].

An analytical methodology was also developed to predict the location and orientation of the first transverse matrix crack based on the principal transverse tension stress distribution in the off axis plies nearest the bondline in the vicinity of the flange tip [7]. Earlier investigations [2,3] indicated that the matrix cracking occurred when the maximum principal transverse tensile stress, σ_{tt}, normal to the fiber direction, as calculated by

$$\sigma_{tt} = \frac{\sigma_{22} + \sigma_{33}}{2} + \sqrt{\left(\frac{\sigma_{22} - \sigma_{33}}{2}\right)^2 + \tau_{23}^2}$$

*ICASE, Mail Stop 132C, NASA Langley Research Center, Hampton, VA 23681-2199, (e-mail: rkrueger@icase.edu). This research was supported by the National Aeronautics and Space Administration under NASA Contract No. NAS1-97046 while the author was in residence at ICASE, NASA Langley Research Center, Hampton, VA 23681-2199.

+ The Boeing Company, Philadelphia, Pennsylvania

reached the transverse tension strength of the material. Here σ_{22} and σ_{33} denote the normal stresses and τ_{23} the shear stress in the 2-3 plane perpendicular to the fiber direction.

A fracture mechanics approach was used to investigate delamination onset once the initial crack had formed. The initial crack was modeled as a discrete discontinuity at a location suggested by the microscopic investigation. The Virtual Crack Closure Technique (VCCT) was used to calculate mixed mode strain energy release rates G_I (due to crack opening), G_{II}, (due to in-plane shear) and G_{III} (due to in-plane scissoring) [8-10]. Computed total strain energy release rates, G_T, were compared to the critical value, G_c, of the material for the appropriate mixed mode ratio (G_{II}/G_T) in order to determine the potential for delamination growth [7].

During previous studies [2-4, 6,7], two-dimensional models were used because they are preferred by industry due to the fact that modeling time, as well as computational time, remains affordable, especially if many different configurations have to be analyzed during the initial design phase. However, it is inherent to any two-dimensional finite element model that the geometry, boundary conditions and other properties are constant across the entire width. The objective of the current study was to evaluate how the results obtained from two-dimensional finite element models of the specimen compared to data obtained from full three-dimensional simulations in order to find the limitations of using simple two-dimensional models. Investigating the limits and usefulness of any numerical model is in general an important engineering science problem that reaches beyond the current analysis of the skin/stringer debond specimen. The present investigation is seen as a contribution to the field complementing earlier studies which focussed on the calculation of energy release rates using different types of finite element models [11, 12].

2. Problem Description. The current study focused on skin-stiffener debonding resulting from buckling of a thin-gage composite fuselage structure as described in reference [7]. In that study, the specimens consisted of a bonded skin and flange assembly as shown in Figure 1(a). An IM7/8552 graphite/epoxy system was used for both the skin and flange. The skin was made of prepreg tape with a measured average ply thickness of h =0.148 mm and had a [45/-45/0/-45/45/90/90/-45/45/0/45/-45] lay-up. The flange was made of a plain-weave fabric with a thickness of h =0.212 mm. The flange lay-up was $[45/0/45/0/45/0/45/0/45]_f$, where the subscript "f" denotes fabric, "0" represents a 0°-90° fabric ply and "45" represents a 0°-90° fabric ply rotated by 45º. The measured bondline thickness averaged 0.178mm. Specimens were 25.4-mm wide and 177.8-mm long. The properties of the graphite/epoxy material and the adhesive were measured at Boeing and are part of the standard design database for the V-22 tilt-rotor aircraft. Typical properties are summarized in Table 1.

Four quasi-static tension tests with a gage length of 101.6 mm were performed as shown in Figure 1(b) [7]. The value of the damage onset load was averaged from four tests and determined to be P =17.8 kN with a coefficient of variation of 8.9%. Three-point bending tests were performed with a bottom support span of 101.6 mm as shown in Figure 1(c). The value of the damage onset load was averaged from four tests and determined to be Q =427.6 kN with a coefficient of variation of 12.8%. The tests were terminated when the flange debonded from the skin. Damage was documented from photographs of the polished specimen edges at each of the four flange corners identified in Figure 1(a). Corners 1 and 4 and corners 2 and 3 showed identical damage patterns for both tests. The damage at corners 2 and 3, formed first and consisted of a matrix crack in the 45º skin surface ply and a

delamination at the +45º/-45º interface as shown in Figure 2. Therefore, this damage pattern was the focus of the current and related earlier analyses [7].

The complex nature of the failure observed during the experiments, where the delamination changed across the specimen width from a delamination running at the skin surface 45°/-45° layer interface to a delamination propagating in the bondline above, suggests the need for a three-dimensional model [7]. Since many layers of brick elements through the thickness would be required to model the individual plies, the size of three-dimensional finite element models, however, may become prohibitively large. Two-dimensional models of a longitudinal cut through the specimen allow for a detailed modeling of the individual plies and the adhesive in thickness direction. Two-dimensional models are preferred by industry due to the fact that modeling time, as well as computational time, remains affordable, especially if many different configurations have to be analyzed during the initial design phase. These models have been used extensively during previous studies [2-4,6,7]. However, it is inherent to any two-dimensional finite element model that the geometry, boundary conditions and other properties are constant across the entire width.

The current study presents an intermediate step where three-dimensional models were created by extruding two-dimensional models across the width. The fact that the delamination changed across the specimen width from a delamination running at the skin surface 45°/-45° layer interface to a delamination propagating in the bondline above, however, is still not accounted for in this model. Nevertheless, the three-dimensional model takes width effects into account and therefore provides insight into the limitations of the use of two-dimensional finite element models. For future detailed modeling and analysis of the damage observed during the experiments, the shell/3D modeling technique [13] offers great potential for saving modeling and computational effort because only a relatively small section in the vicinity of the delamination front needs to modeled with solid elements.

The objective of the current study was to evaluate how the assumptions made in developing two-dimensional finite element models of the specimen would effect the damage onset prediction for skin-stiffener debonding. Geometrically nonlinear finite element analyses were performed using ABAQUS® two-dimensional plane-stress, plane-strain and generalized plane strain elements. Additionally, two different methods to create generalized plane strain conditions were studied [11,14]. The results were compared to data obtained from full three-dimensional simulations to study the feasibility and limitations of using simple two-dimensional models. Computed deflections, transverse tensile stresses in the skin surface 45° layer, flange and skin strains, as well as mixed mode strain energy release rates were compared.

3. Analysis Formulation

3.1. Two-Dimensional Finite Element Models. Several assumptions are possible in two-dimensional models. A plane-stress model imposes the out of plane stresses to be zero ($\sigma_{zz}=\tau_{xz}=\tau_{yz}=0$) at the free edge of each ply and allows the displacement to be the free parameter. The plane-strain model, on the other hand, imposes the out of plane strains to be zero ($\varepsilon_{zz}=\gamma_{xz}=\gamma_{yz}=0$) at the free edge, which excessively constrains the plies. Hence, the two dimensional plane stress and plane strain conditions may serve as upper and lower limits compared to the three-dimensional solution.

An outline of the two-dimensional model of the specimen showing the boundary conditions, and loads applied is shown in Figure 3. Finite element models for an undamaged and a damaged specimen were developed using a refined mesh in the critical area of the 45° skin ply where cracking was observed during the tests. Outside the mesh refinement area, all plies were modeled with one element through the ply thickness. In the refined region, four elements were used per ply thickness for the first two individual flange plies above the bondline and the top skin ply below the bondline as shown in Figures 3(b) and (c) and described in more detail in reference [7]. Four elements through the thickness were also used to model the adhesive film. Ply properties and adhesive material properties used in this study are summarized in Table 1.

Damage in the form of a matrix crack in the top 45° skin ply that developed into a delamination in the 45°/–45° interface is shown in Figure 2. Delaminations of various lengths were modeled by discrete discontinuities as shown in Figure 3(c). The delamination propagating in a bimaterial interface (45°/-45°) may, for small element lengths Δa at the crack tip, result in incorrect mode separation of the total energy release rate. This effect is caused by the oscillatory singularity at the crack tip [15]. To avoid the effect, for the current investigation the element length Δa was chosen to be about 1/3 of the ply thickness. At the opposite taper, the original mesh created for the model of the undamaged specimen was used. Finite element solutions were obtained using the commercial ABAQUS®/Standard finite element software. Eight-noded quadrilateral plane-stress (CPS8R) and plane-strain (CPE8R) elements with quadratic shape functions and a reduced (2x2) integration scheme were utilized for the geometric nonlinear analyses [16].

3.2. Generalized Plane Strain Models. One alternative to a full three-dimensional simulation that requires about the same modeling effort as the simple two-dimensional models is a generalized plane-strain model. Generalized plane strain elements provided by ABAQUS® code are typically used to model a section of a long structure that is free to expand or is subjected to loading perpendicular to the plane of modeling. The formulation involves a model that lies between two planes that can move with respect to each other, and hence, cause strain in the direction perpendicular to the plane of the model that varies linearly with respect to position in the planes [16]. Ten-noded quadrilateral generalized plane-strain (CGPE10R) elements with quadratic shape functions and a reduced (2x2) integration scheme were used in the current models. The models shown in Figure 2 were modified to use generalized plane strain analysis. Each element was assigned two additional nodes, which determined the position of the bounding planes and were common to all the elements.

A different approach to create a generalized plane strain case was suggested by Minguet [14]. The generalized plane-strain case is regarded as an intermediate state between plane strain and plane stress, and assumes that the out of plane normal strain $\varepsilon_{zz}=-\nu_L\varepsilon_{xx}$, where ν_L is the laminate Poisson's ratio, and the shear strain $\gamma_{xz}=\gamma_{yz}=0$. With these assumptions, ply stiffnesses were calculated for each ply angle in the specimen and entered as material properties for the two-dimensional models shown in Figure 3. Details are given in appendix A. Eight-noded quadrilateral plane-stress (CPS8R) elements with quadratic shape functions and a reduced (2x2) integration scheme were used for this analysis.

Another possibility to create a two-dimensional generalized plane strain model was described by König [11]. The model is obtained by using one row of three-dimensional brick elements instead of plate, shell or membrane

elements. Therefore, the two-dimensional models shown in Figures 3(b) and (c) were extruded into the models shown in Figures 4(b) and (c). This resulted in a 0.1 mm wide model made of one row of brick elements (C3D20R) with quadratic shape functions and a reduced integration scheme. The advantage of this model is the inclusion of three-dimensional effects in this two-dimensional finite element model. However, the number of degrees of freedom almost quadruple in comparison with membrane elements. The model may be compared to a wall, where one side of the model represents the midplane and the other side is a parallel plane. The midplane of the specimen as shown Figure 4(b) is a plane of symmetry and remains plane under the applied load. The displacements perpendicular to the plane are surpressed (w=0) at all nodes in the midplane. All displacements in the z-direction at the nodes of the parallel plane are coupled to a constant value w. In ABAQUS® the coupling is achieved by grouping all nodes in the parallel plane except for one. The w displacement of all the nodes grouped is then set equal to the w displacement of the one node not included in the group using a linear constraint equation. These coupled displacements at the parallel plane will generate stress resultants at each node of this plane, but the summation of these stress resultants has to vanish because of the zero load in this direction.

3.3. Three-Dimensional Finite Element Model. The three-dimensional model of the specimen with load and boundary conditions is shown in Figure 5 for the tension and in Figure 6 for the three-point bending load case. The specimen was modeled with ABAQUS® solid twenty-noded hexahedral elements C3D20R with quadratic shape functions and a reduced integration scheme. A two-dimensional mesh was made first in the x-y plane, which was then extruded across the width to create the model shown in Figure 5.

The same refined mesh as in the two-dimensional model (Figure 3) was used in the critical area of the 45° skin ply where cracking was observed during the tests. Outside the refined area, the mesh was modified to prevent the three-dimensional model from becoming excessively large Figure 5(b). The skin plies were grouped into three layered elements with -45/45/90, 90/-45/45 and 0/45/-45 respectively, thus taking advantage of the composite solid element option in ABAQUS® [16]. The fabric layers were grouped into two layered elements as shown in Figure 5(b). In the transition region at the flange several plies were modeled by one element with material properties smeared using the rule of mixtures [17]. This procedure used did not ensure the full A-B-D contribution of the plies, however, appeared suitable for the small transition region to enforce a reasonable model size.

For the stress analysis the two-dimensional model was extruded into twenty elements across the width of the specimen, with a refined zone (0.74 mm, five elements) near the free edges (z=0.0 mm and z=25.4 mm) as shown in Figures 5(a) and (b). This resulted in a model with 64,180 elements and 279,842 nodes yielding at total of 839,526 degrees of freedom. The nonlinear analysis required about 50 hours of CPU time on a *SGI Origin 3200* workstation. The fracture mechanics approach requires multiple analyses to calculate the energy release rate for many different delamination lengths to obtain a distribution plot. Due to the large computation time required for each analysis it was decided to use a smaller model. The two-dimensional model was extruded into only ten elements across the width of the specimen as shown in Figures 5(6) and 6. The final model had 32,090 elements, 145,432 nodes yielding at total of 436,296 degrees of freedom and required only about eight hours of CPU time on the same workstation. This three-dimensional mesh, however, is not fine enough in the vicinity of the free edges (z=0.0 mm

and z=25.4 mm) to accurately capture the influence of the free edges on the distribution of the energy release rates across the width.

For future detailed modeling and analysis of the damage observed during the experiments, the shell/3D modeling technique [13] offers great potential for saving modeling and computational effort because only a relatively small section in the vicinity of the delamination front needs to modeled with solid elements. However, the applicability of the shell/3D modeling technique to the skin/stiffener debond problem needs to be assessed first. The scope of the current paper therefore was limited to the comparison of results obtained from different two-dimensional models to data obtained from full three-dimensional analysis and resulting recommendations.

4. Analytical Investigation

4.1. Global Response. First, the global response of the specimens was computed at the mean quasi-static damage onset load determined from experiments. The load-displacement and the load-strain behavior computed from different FE models were compared to the corresponding experimental results. This global response was used to examine whether the FE models, the boundary conditions, the loads and the material properties used in the model yielded reasonable results. Strains were averaged from computed nodal point values over a length corresponding to the dimensions of the strain gages shown in Figure 1(a) [7].

A schematic of the deformed geometry, the boundary conditions, and the load applied in the simulations is shown in Figure 3(a) for the tension load case. In the schematic, the elongation of the specimen caused by the applied tensile load is shown. The bending effect caused by the load eccentricity in the flange region, the asymmetric layup with respect to the neutral axis, and the membrane stiffening effect is also shown. For the specimen subjected to three-point bending the deformed three-dimensional model, the boundary conditions, and the load applied in the simulations are shown in Figure 6(a). A detail of the modeled delaminated region is shown in Figure 6(b). For short delamination lengths (a < 1.0 mm) crack opening mode I was apparent. For longer delaminations mode I ceased and the surfaces started to overclose as shown in the detail of Figure 6(c). This phenomenon was not observed in the results from two-dimensional analyses.

4.1.1 Tension Test. The load versus displacement plot in Figure 7 shows that plane-strain model exhibited a stiffer behavior than the experiments yielding an upper bound while the plane-stress models were more compliant yielding a lower bound. The results from two of the generalized plain strain cases and the full three-dimensional model fall between the results from the plane stress and plane strain and agree best with the experimental results. The generalized plain strain model suggested by König studied [11] yields results similar to the plane stress model.

A comparison of measured strains at the surface of the flange (see Figure 1(a)) and computed results is shown in Figure 8. The plane-strain model was stiffer, yielding an upper bound, and the plane-stress model was more compliant, yielding a lower bound compared to the results from the other models. The results from the generalized plain strain models and the full three-dimensional model agree best with the strain recorded during the tests.

In Figure 9, measured strains at the surface of the top 45º skin ply near the flange tip (see Figure 1(a)) and computed surface strains were compared. Scatter in the experiments can not be shown as only one test was equipped

with a strain gage on the skin. As mentioned above, the plane-strain models showed a stiffer behavior and the plane-stress models a more compliant behavior compared to the tested specimen. The results from two of the generalized plain strain cases and the full three-dimensional model fall between the results from the plane stress and plane strain simulation, however, appear stiffer when compared to this single test. The generalized plain strain model suggested by König [11] yields results similar to the plane stress model.

4.1.2 Three-Point Bending Test. The load versus displacement plot in Figure 10 shows that plane-strain model exhibited a stiffer behavior than the experiments (DCDT) yielding an upper bound while the plane-stress models were more compliant yielding a lower bound. The results from two of the generalized plain strain cases and the full three-dimensional model fall between the results from the plane stress and plane strain and agree best with the experimental results. The generalized plain strain model using the ABAQUS® CGPE10R elements yields results similar to the plane strain model.

A comparison of measured strains at the surface of the flange (see Figure 1(a)) and computed results is shown in Figure 11. The plane-strain model was stiffer yielding an upper bound, and the plane-stress models more compliant yielding a lower bound compared to the results from the other models. The results from the generalized plain strain models and the full three-dimensional model fall between these two results, however are consistently lower than the experimental results.

In Figure 12, measured strains at the surface of the top 45º skin ply near the flange tip (see Figure 1(a)) and computed surface strains were compared. As mentioned above, the plane-strain model showed a stiffer behavior and the plane-stress model a more compliant behavior compared to the tested specimen. The results from two of the generalized plain strain cases and the full three-dimensional model fall between the results from the plane stress and plane strain simulation. The generalized plain strain model suggested by König [11] yields results closer to the plane stress model. The generalized plain strain model using the ABAQUS® CGPE10R elements yields results similar to the plane strain model.

In the global response analysis, the load-displacement and the strain-load behavior computed for the tension and the three-point bending load cases were compared to the corresponding experimental results. The slightly stiffer response of the full three-dimensional model numerical model may be explained by the fact that the material data used in the FE simulation originate from the literature. For a consistent simulation, material data should be taken from the batch of material that was used to manufacture the specimens. Results from the plane-strain analysis indicated a stiffer behavior as expected. This is caused by the constraints inherent to the plane-strain model, particularly in the ±45° plies. The plane-stress model which imposes the out of plane stresses to be zero and allows the displacement to be the free parameter exhibits – as expected - a more compliant behavior. The stiffnesses of the generalized plain strain models fall between the stiffnesses from the plane stress and plane strain assumptions.

4.2. Local Response

4.2.1 Stress Analysis. A stress analysis was used to study the initial damage in the form of matrix cracking. The maximum principal tensile stress, σ_{tt}, normal to the fiber direction was calculated for the static failure load using the two-dimensional and three-dimensional finite element models introduced in the previous section. The

stress distribution in the top 45º skin ply is plotted in the immediate vicinity of the flange tip in Figures 13 and 14 for the tension and bending tests respectively. In the graph, x=0 mm corresponds to left grip as shown in Figures 2 to 4, and x=26.4 mm corresponds to the left flange tip. During the fatigue tests, first matrix cracking was observed at locations right next to the flange tip which corresponds to the location where peak stresses were calculated [7].

The transverse tensile strength and scatter band, for IM7/8552, obtained from three-point bending tests of 90° lamina, were added to the plot for comparison [18]. Stresses at the static failure load computed from the plane-stress analysis correspond with the transverse tensile strength. Stresses from the plane-strain analysis are excessively high. This is caused by the constraints inherent to the plane-strain model, particularly in the ±45° plies. Plots of the three-dimensional stress distribution across the width of the specimen are shown in Figures 15 and 16. The stress distribution has a maximum at x=26.6 mm with a peak in the center of the specimen (z=12.7 mm). The computed stress drops off towards the edges before it sharply increases near the free edges (z=0.0 mm and z=25.4 mm). A locally even more refined mesh would be required to capture further details near the edges.

4.2.2 Fractures Mechanics Analysis. A fracture mechanics approach was used to investigate delamination onset once the initial crack had formed. During a series of nonlinear finite element analyses, strain energy release rates were computed at each front location for the loads applied in the experiments. A critical energy release rate, G_c, needs to be determined to predict delamination onset. This critical G is generally identified based on the shape of the total energy release rate versus delamination length curve, which is determined through analysis as shown in Figures 17 and 18. The G_T versus x curve reached a peak at some virtual delamination length and then decreased. The delamination was extended to a total simulated length of 2.2 mm to ascertain that the peak value had been captured.

The total energy release rates computed for all two-dimensional and generalized plane strain models are plotted in Figures 17 and 18. The values obtained from three-dimensional analysis along the centerline of the specimen (z=12.7 mm) was included in Figures 17 and 18. Qualitatively, all results follow the same trend. After a small initial drop the computed total energy release rate increases sharply with delamination length, reaches a peak value and gradually decreases. As expected the values from plane stress and plane strain analysis form an upper and lower bound, except for very short delamination lengths. Results from generalized plane strain models and the three-dimensional model fall between the results from two-dimensional analysis. The generalized plain strain model suggested by König [11] yields results closer to those obtained from the plane stress model. All generalized plane strain peak G_T results are within 8.5% of the results obtained from full three-dimensional analysis at the center of the specimen.

Unlike the tension loading case, the G_T versus x curves are continuously increasing, indicating unstable delamination growth. Qualitatively all results follow the same trend. As before the values from plane strain analysis form an upper, except for very short delamination lengths. The generalized plain strain model using the ABAQUS® CGPE10R elements yields results similar to the plane strain model and yields a lower bound. For larger delamination lengths (a > 0.5 mm) the other generalized plane strain models yield G_T results are within 6% of the results obtained from full three-dimensional analysis at the center of the specimen.

Three-dimensional plots of the distribution of the energy release rate across the width of the specimen are shown in Figures 19 and 20. Values at the free edge (z=0.0 mm and z=25.4 mm) have been excluded from the plots as the model was not fine enough to accurately capture the influence of the free edges on the distribution of the energy release rates. Along the length (x-coordinate) it was observed for the tension case that after a small initial drop the computed total energy release rate increases sharply with delamination length, reaches a peak values and gradually decreases. Across the width (z-coordinate) the computed total energy release rate gradually increases with z before it drops off near the free edge (z=25.4 mm). Unlike the tension loading case, G_T increases continuously along the length (x-coordinate), except for the zones near the free edges (z=0.0 mm and z=25.4 mm) where a sharp decrease is observed caused by the overclosure of the interfaces after about 1 mm of delamination growth. Across the width (z-coordinate) the computed total energy release rate gradually increases with z before it drops off near the free edge (z=25.4 mm).

The variation of mixed mode ratio G_S/G_T with delamination length is shown in Figures 21 and 22. Here G_S denotes the sum of the in-plane shearing components $G_{II}+G_{III}$, and G_T denotes the total energy release rate $G_I+G_{II}+G_{III}$, where G_I is the opening mode. For two-dimensional analyses, where G_{III}=0, this definition is equal to the previously used definition of the mixed mode ratio, G_{II}/G_T. For three-dimensional analysis, which also yields results for the scissoring mode G_{III}, the modified definition of G_S is introduced.

For the tension load all analyses yield the same trend, where the delamination initially starts with high shearing components, followed by a drop which is equivalent to an increase in G_I. For longer delaminations a gradual increase in shearing components is observed. For a more realistic comparison of the G_{II} contribution from two-dimensional and three-dimensional models results from the three-dimensional analysis were calculated assuming G_S=G_{II} and ignoring G_{III}. As Figure 21 shows, these results fall between the results from two-dimensional analysis, for longer delamination lengths. For G_S=G_{II}+G_{III}, the contribution of the in-plane shearing component is larger compared to the mode ratios obtained from two-dimensional analysis.

For the three-point bending load case all analyses yield the same trend as before, where the delamination initially starts with high shearing components, followed by a drop which is equivalent to an increase in opening mode I. For longer delaminations the shearing component remains constant. For the case where G_S=G_{II} was chosen, the results from three-dimensional analysis in the center of the specimen (z=12.7 mm) show a higher shearing component compared to the results from two-dimensional analysis. For the other case (G_S=G_{II}+G_{II}) the contribution of the shearing component is even larger compared to the mode ratios obtained from two-dimensional analysis. This may be an effect caused by the overclosure of the delaminated surfaces observed near the edges in the three-dimensional model. A detailed study of this phenomenon would require contact analysis and preferably a refined model near the free edges.

Three-dimensional plots of the distribution of the energy release rate across the width of the specimen are shown in Figures 23 and 24. Values at the free edge (z=0.0 mm and z=25.4 mm) have been excluded from the plots as the model was not fine enough to accurately capture the influence of the free edges on the distribution of the energy release rates. Along the length (x-coordinate) it was observed for the tension case that the delamination initially starts with high shearing components, followed by a drop which is equivalent to an increase in opening

mode I. For longer delaminations a gradual increase in shearing components is observed. Across the width (z-coordinate) the computed mixed mode ratio drops slightly. For the three-point bending load case it was observed along the length (x-coordinate) that the delamination initially starts with high shearing components, followed by a drop which is equivalent to an increase in opening mode I. For longer delaminations the shearing component remains constant. Unlike the tension loading case, the mixed mode ratio rises sharply at the edges for delaminations longer than 1 mm. This is caused by the overclosure of the delaminated surface near the edges where the crack opening mode I disappears.

5. Concluding Remarks. The influence of the assumptions made in developing two-dimensional finite element models on skin-stiffener debonding specimens was studied. Geometrically nonlinear finite element analyses using two-dimensional plane-stress and plane-strain elements as well as three different generalized plane strain type approaches were performed. The computed skin and flange strains, transverse tensile stresses and energy release rates were compared to results obtained from three-dimensional simulations.

The plane stress and plane strain models provided results for skin and flange strains, as well as energy release rates, which form an upper and lower bound of the results obtained from full three-dimensional analysis. The results from generalized plane strain models fall between the results obtained from plane stress and plane strain models. The generalized plane strain models capture the surface strains on the flange and skin very well. Computed energy release rates are within 9% of the results from three-dimensional analysis, however, there is not consistency across the load cases with respect to which model performs best. Stresses obtained from plane strain and generalized plane strain models, were excessively high when compared to results from three-dimensional analysis. The stresses from full three-dimensional analysis were lower than results from any of the two-dimensional models, but are closest to the plane stress results.

In general, two-dimensional models are preferred by industry because modeling time, as well as computational time, remains affordable, especially if many different configurations have to be analyzed during the initial design phase. The effect of two-dimensional modeling assumptions is most marked for 45° plies because of their high in-plane Poisson's ratio, while it is small for 0° and 90°. Based on the results of this investigation – which contains 45° tape and fabric plies - it is recommended to use results from plane stress and plane strain models as upper and lower bounds. Two-dimensional models may also be used to qualitatively evaluate the stress distribution in a ply and the variation of energy release rates and mixed mode ratios with delamination length. The current recommendations are based on the analysis of the skin/stringer specimen with the described layup. Further analyses are required before the recommendations may be generalized.

Acknowledgements. The authors gratefully acknowledge Drs. T. Kevin O'Brien and Isabelle Paris for providing insight and experimental results on the specimens analyzed in this paper. The authors would also like to thank Prof. Barry D. Davidson of Syracuse University, D. M. Hoyt of NSE Composites and Dr. Manfred König of the University of Stuttgart for the discussions about generalized plane strain assumptions.

Appendix A

Generalized Plane Strain Procedure. The difficulty in using two-dimensional modeling when representing laminated composites is that although the laminate may be in a state of plane stress, each lamina is typically not a state of plane stress. The effect is most marked for 45° plies because of their high in-plane Poisson's ratio, while it is small for 0° and 90°. There does not appear to be an exact solution to this problem, however the following procedure is an approach that represents a compromise between accuracy and efficiency of two-dimensional modeling.

The traditional three-dimensional stress-strain relationships with the traditional orientations as shown in Figure A1 where x, y, and z are the laminate axes and 1, 2, and 3 the lamina axes can be written as

$$\sigma = \begin{bmatrix} \sigma_{xx} \\ \sigma_{yy} \\ \sigma_{zz} \\ \tau_{yz} \\ \tau_{xz} \\ \tau_{xy} \end{bmatrix} \qquad \varepsilon = \begin{bmatrix} \varepsilon_{xx} \\ \varepsilon_{yy} \\ \varepsilon_{zz} \\ \gamma_{yz} \\ \gamma_{xz} \\ \gamma_{xy} \end{bmatrix} \qquad \sigma = [E]\,\varepsilon \qquad \varepsilon = [C]\,\sigma$$

where σ_{ij} and τ_{ij} denote the normal and shear stresses and ε_{ij} and γ_{ij} the normal and shear strains respectively. In the matrix formulation $[E]$ denotes the 6x6 stiffness matrix and $[C]$ the 6x6 compliance matrix.

The two traditional two-dimensional assumptions are plane strain, where $\varepsilon_{yy}=\gamma_{xy}=\gamma_{yz}=0$ and plane stress, where $\sigma_{xx}=\tau_{xy}=\tau_{yz}=0$. An intermediate state is proposed here where is assumed that: $\varepsilon_{yy}=-\nu_L\varepsilon_{xx}$ and $\gamma_{xy}=\gamma_{yz}=0$, where ν_L is a laminate Poisson's ratio.

Applying this assumption yields:

$$\begin{aligned} \sigma_{xx} &= E_{11}\varepsilon_{xx} - \nu_L E_{12}\varepsilon_{xx} + E_{13}\varepsilon_{zz} \\ \sigma_{zz} &= E_{31}\varepsilon_{xx} - \nu_L E_{32}\varepsilon_{xx} + E_{33}\varepsilon_{zz} \\ \tau_{xz} &= E_{55}\gamma_{xz} \end{aligned}$$

$$\text{or} \quad \sigma = \left[E^*\right]\varepsilon \quad \text{and} \quad \varepsilon = \left[C^*\right]\sigma \quad \text{where} \quad \left[C^*\right] = \left[E^*\right]^{-1}$$

The following lamina moduli are then extracted and used as input for a two-dimensional finite element model to be run as a plane stress model:

$$E_{xx} = \frac{1}{C_{11}^*} \qquad E_{zz} = \frac{1}{C_{22}^*} \qquad \upsilon_{xz} = -\frac{C_{12}^*}{C_{11}^*} \qquad G_{xz} = \frac{1}{C_{33}^*}$$

The results from the two-dimensional finite element analysis need to be post-processed to recover the transverse stresses at the lamina level.

$$\varepsilon_{yy} = -\upsilon_L \varepsilon_{xx}$$
$$\varepsilon_{zz} = C_{21}^* \sigma_{xx} + C_{22}^* \sigma_{zz}$$
$$\sigma_{yy} = E_{21}\varepsilon_{xx} + E_{22}\varepsilon_{yy} + E_{23}\varepsilon_{zz}$$
$$\tau_{xy} = E_{61}\varepsilon_{xx} + E_{62}\varepsilon_{yy} + E_{63}\varepsilon_{zz}$$

Once the lamina stresses have recovered, they are rotated into lamina axes. The maximum transverse stress is then calculated in the transverse 2-3 plane as shown in Figure A2:

$$\sigma_{tt} = \frac{\sigma_{22} + \sigma_{33}}{2} + \sqrt{\left(\frac{\sigma_{22} - \sigma_{33}}{2}\right)^2 + \tau_{23}^2}$$

REFERENCES

[1] P. J. MINGUET, M. J. FEDRO, T. K. O'BRIEN, R. H. MARTIN, AND L. B. ILCEWICZ, *Development of a Structural Test Simulating Pressure Pillowing Effects in Bonded Skin/Stringer/Frame Configuration*, in Proceedings of the Fourth NASA/DoD Advanced Composite Technology Conference, Salt Lake City, Utah, 1993.

[2] P. J. MINGUET AND T. K. O'BRIEN, *Analysis of Test Methods for Characterizing Skin/Stringer Debonding Failures in Reinforced Composite Panels*, in Composite Materials: Testing and Design (Twelfth Volume), ASTM STP 1274, 1996, pp. 105-124.

[3] P. J. MINGUET AND T. K. O'BRIEN, *Analysis of Composite Skin/Stringer Bond Failures Using a Strain Energy Release Rate Approach*, in The Tenth International Conference on Composite Materials, vol. I, A. Poursartip and K. Street, Eds., 1995, pp. 245-252.

[4] P. J. MINGUET, *Analysis of the Strength of the Interface Between Frame and Skin in a Bonded Composite Fuselage Panel*, in The 38rd AIAA/ASME/ASCE/AHS/ASC Structures, Structural Dynamics and Materials Conference, 1997, pp. 2783-2790.

[5] M. K. CVITKOVICH, T. K. O'BRIEN, AND P. J. MINGUET, *Fatigue Debonding Characterization in Composite Skin/Stringer Configurations*, in Composite Materials: Fatigue and Fracture, Seventh Volume, ASTM STP 1330: American Society for Testing and Materials, 1998, pp. 97-121.

[6] R. KRUEGER, M. K. CVITKOVICH, T. K. O'BRIEN, AND P. J. MINGUET, *Testing and Analysis of Composite Skin/Stringer Debonding Under Multi-Axial Loading*, Journal of Composite Materials, 34, (2000), pp. 1263-1300.

[7] R. KRUEGER, I. L. PARIS, T. K. O'BRIEN, AND P. J. MINGUET, *Fatigue Life Methodology for Bonded Composite Skin/Stringer Configurations*, NASA-TM-2001-210842, 2001.

[8] E. F. RYBICKI AND M. F. KANNINEN, *A Finite Element Calculation of Stress Intensity Factors by a Modified Crack Closure Integral*, Eng. Fracture Mech., 9, (1977), pp. 931-938.

[9] I. S. RAJU, *Calculation Of Strain-Energy Release Rates With Higher Order And Singular Finite Elements*, Eng. Fracture Mech., 28, (1987), pp. 251-274.

[10] F. G. BUCHHOLZ, H. GREBNER, K. H. DREYER, AND H. KROME, *2D- and 3D- Applications of the Improved and Generalized Modified Crack Closure Integral Method*, in Computational Mechanics '88, S.N. Atluri, and G. Yagawa, Eds., 1988.

[11] M. KÖNIG, R. KRÜGER, E. KOHLER, M. KURZ, AND T. RUCKSTUHL, *Analytical and Numerical Analysis of a Specimen Containing a Delamination Caused by a Ply Cut*, Institute for Statics and Dynamics of Aerospace Structures, University of Stuttgart ISD-Report No. 97/2, Rev. B, 1999.

[12] R. KRÜGER, *Three Dimensional Finite Element Analysis of Multidirectional Composite DCB, SLB and ENF Specimens*, Institute for Statics and Dynamics of Aerospace Structures, University of Stuttgart ISD-Report No. 94/2, 1994.

[13] R. KRUEGER AND T. K. O'BRIEN, *A Shell/3D Modeling Technique for the Analysis of Delaminated Composite Laminates*, Composites Part A: Applied science and manufacturing, 32, (2001), pp. 25-44.

[14] D. M. HOYT, S. H. WARD, AND P. J. MINGUET, *Strength and Fatigue Life Modeling of Bonded Joints in Composite Structure*, in Proceedings of the American Society for Composites - 15th Annual Technical Conference on Composite Materials: Technomic Publishing, 2000, pp. 729-736.

[15] I. S. RAJU, J. H. CREWS, AND M. A. AMINPOUR, *Convergence of Strain Energy Release Rate Components for Edge-Delaminated Composite Laminates*, Eng. Fracture Mech., 30, (1988), pp. 383-396.

[16] *ABAQUS/Standard - User's Manual - Version 5.6*, vol. II: Hibbitt, Karlsson & Sorensen, Inc., 1996.

[17] S. W. TSAI AND H. T. HAHN, *Introduction to Composite Materials*, Technomic Publishing Co., Inc., 1980.

[18] T. K. O'BRIEN, A. D. CHAWAN, K. DEMARCO, AND I. L. PARIS, *Influence of Specimen Preparation and Specimen Size on Composite Transverse Tensile Strength and Scatter*, NASA/TM-2001-211030, ARL-TR-2540, 2001.

TABLE 1.

Material Properties

IM7/8552 Unidirectional Graphite/Epoxy Prepreg		
E_{11} = 161.0 GPa	E_{22} = 11.38 GPa	E_{33} = 11.38 GPa
ν_{12} = 0.32	ν_{13} = 0.32	ν_{23} = 0.45
G_{12} = 5.17 GPa	G_{13} = 5.17 GPa	G_{23} = 3.92 GPa
IM7/8552 Graphite/Epoxy Plain Weave Fabric		
E_{11} = 71.7 GPa	E_{22} = 71.7 GPa	E_{33} = 10.3 GPa
ν_{12} = 0.04	ν_{13} = 0.35	ν_{23} = 0.35
G_{12} = 4.48 GPa	G_{13} = 4.14 GPa	G_{23} = 4.14 GPa
Grade 5 FM300 Adhesive		
E = 1.72 GPa	ν = 0.3	(assumed isotropic)

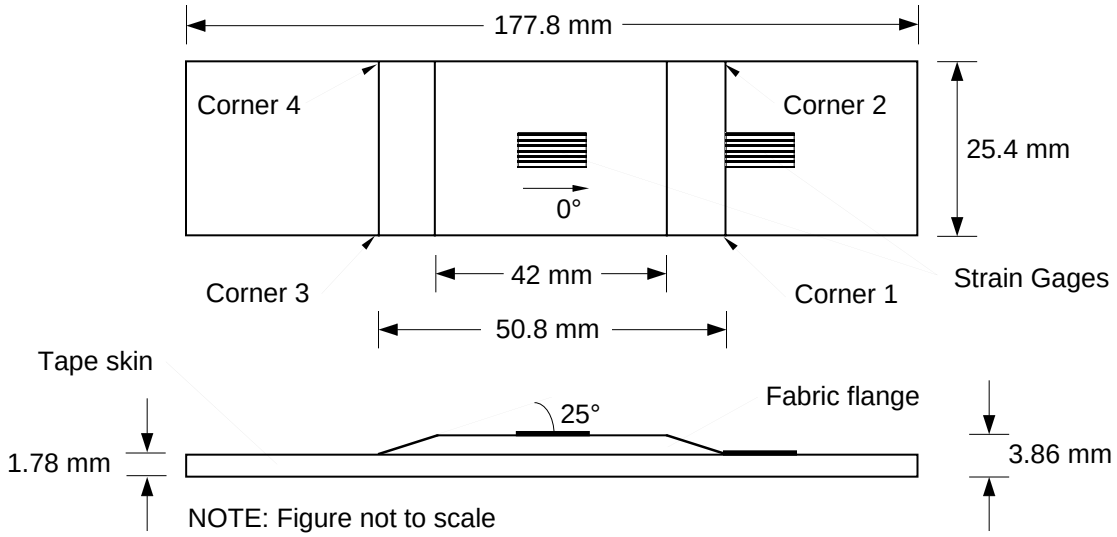

(a) Specimen configuration

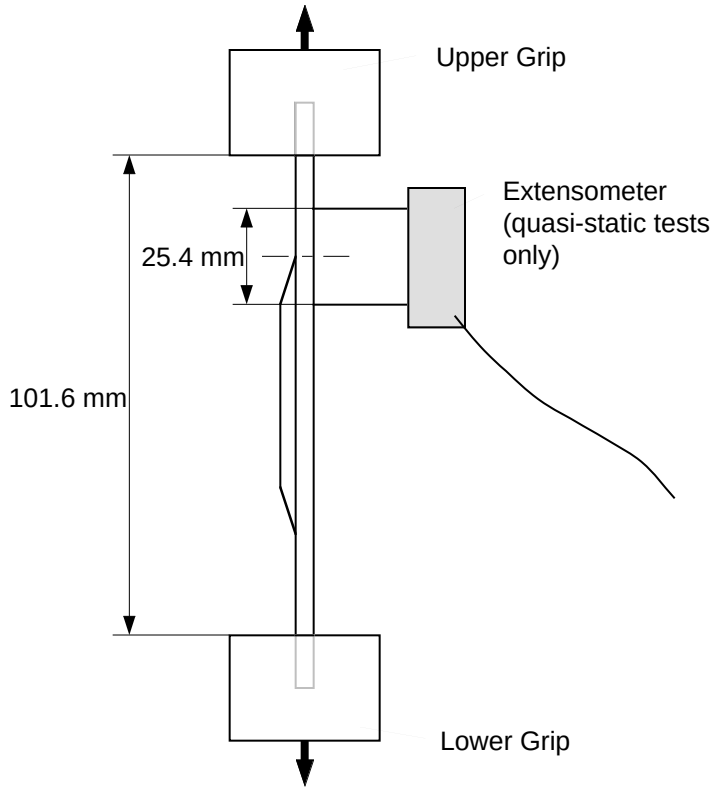

(b) Tension test set-up

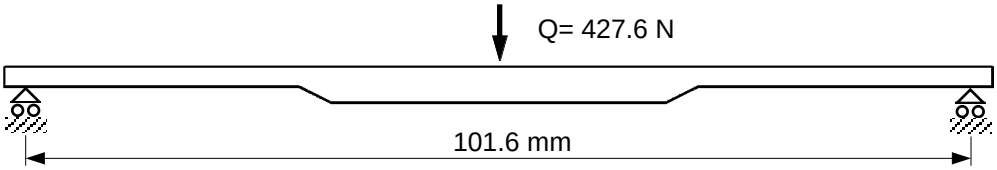

(b) Three-point bending case

FIGURE 1. *Specimen configuration and test set-up*.

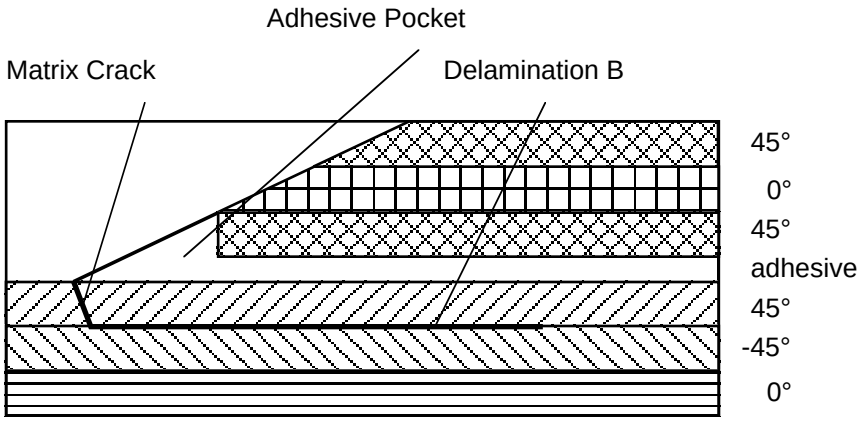

FIGURE 2. *Typical damage patterns at specimen corners 2 and 3 [7]*

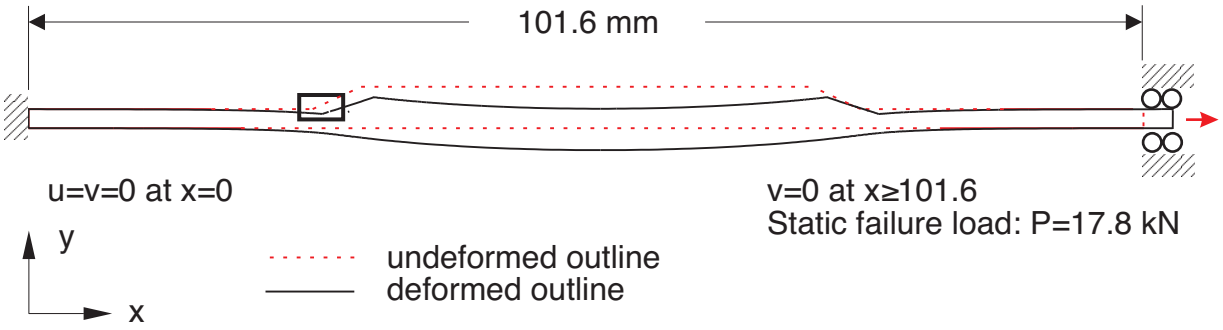

(a) Outline of model with load and boundary conditions

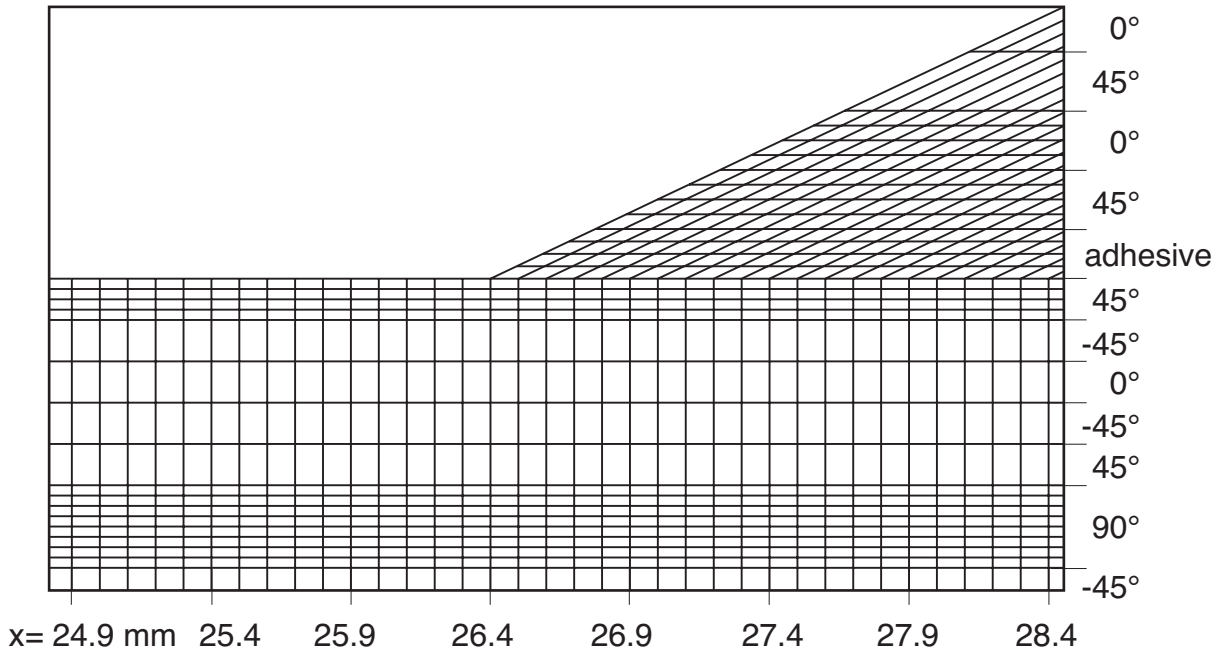

(b) Detail of model of undamaged specimen

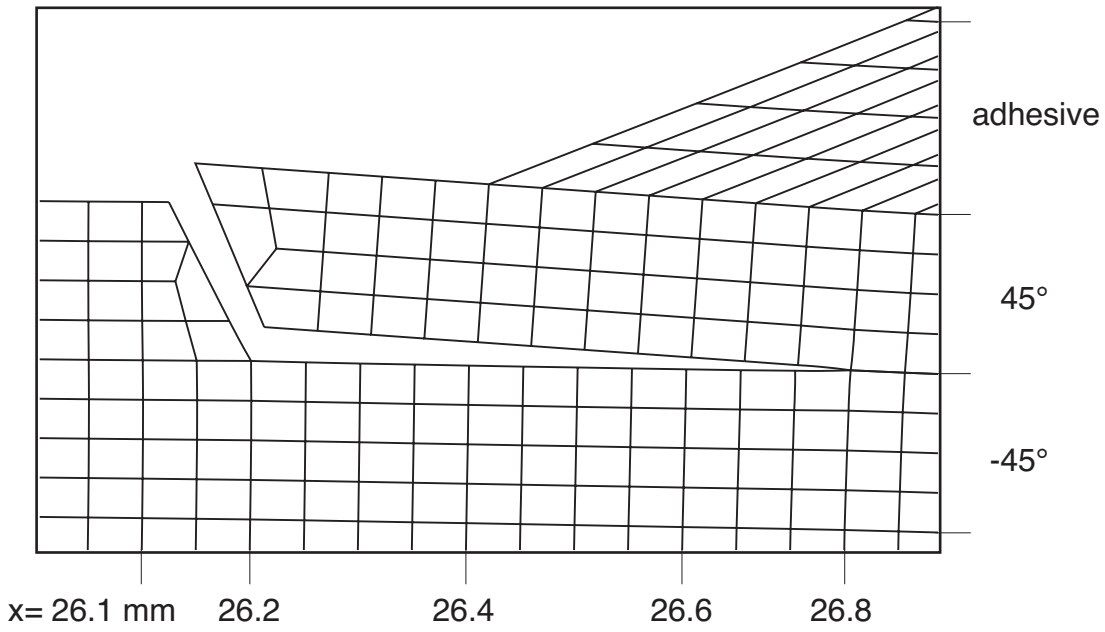

(c) Detail of deformed model of damaged specimen

FIGURE 3. *Two dimensional finite element model of skin/flange specimen*

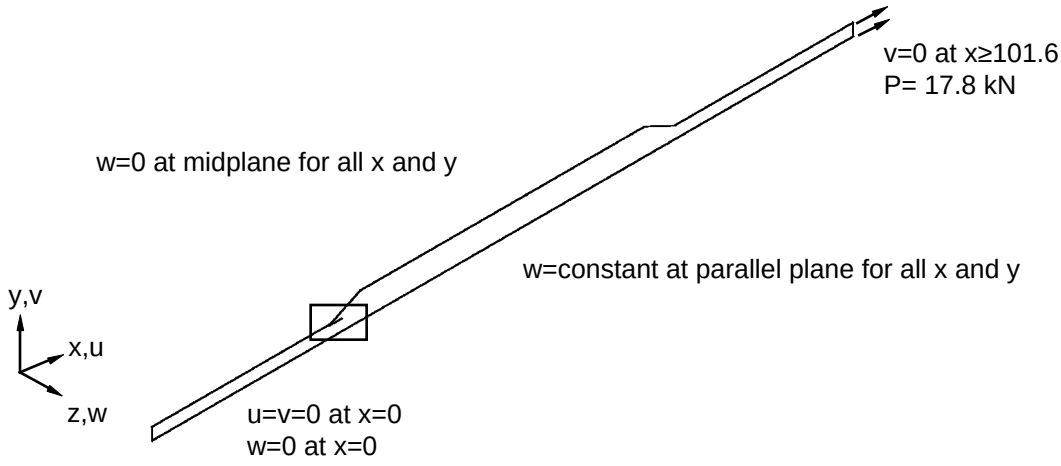

(a) Three-dimensional plane strain model with load and boundary conditions

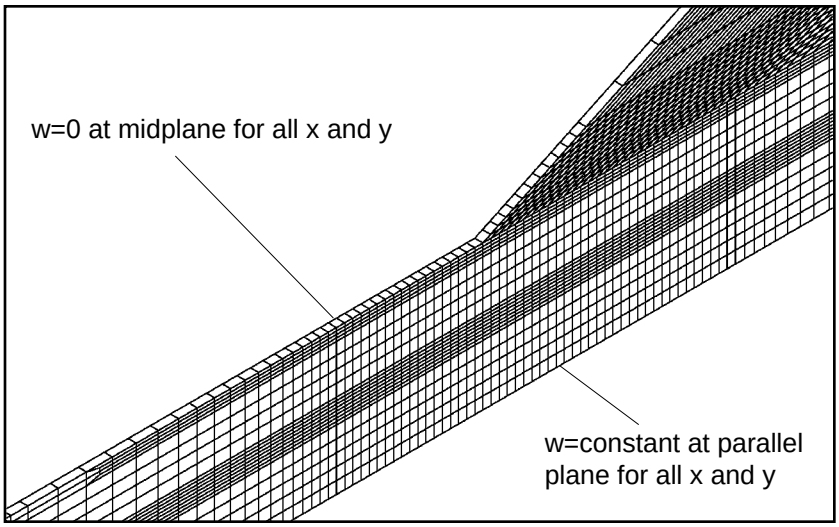

(b) Detail of model of undamaged specimen

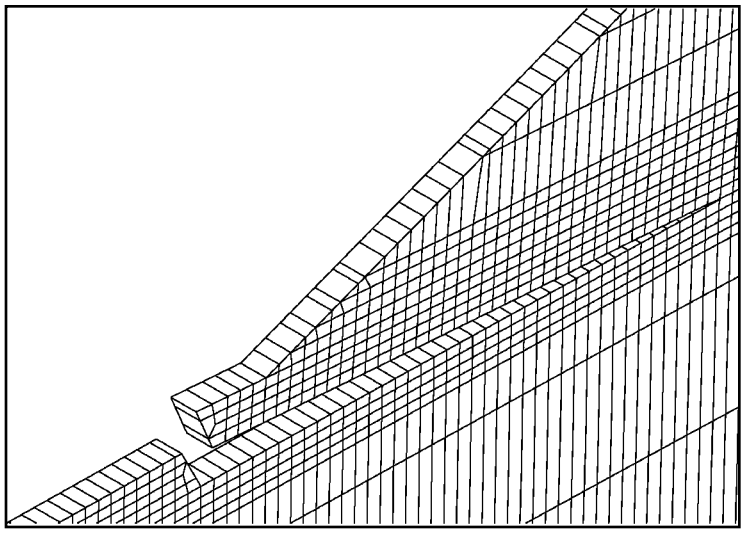

(c) Detail of deformed model of damaged specimen

FIGURE 4. *Three-dimensional generalized plane strain model of skin/flange specimen*

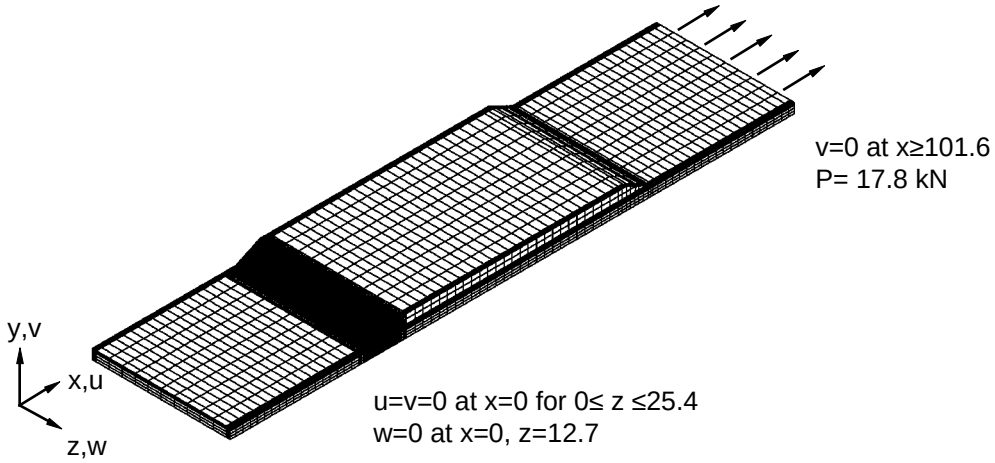

(a) Three-dimensional model with load and boundary conditions

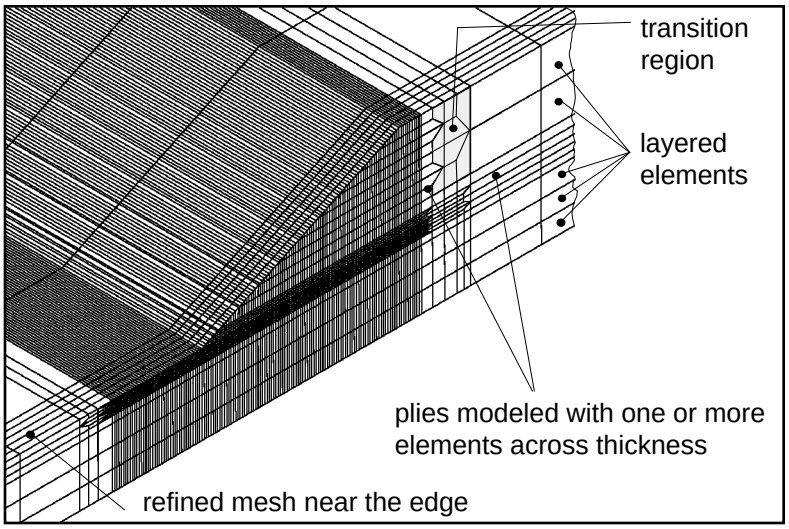

(b) Detail of model of undamaged specimen

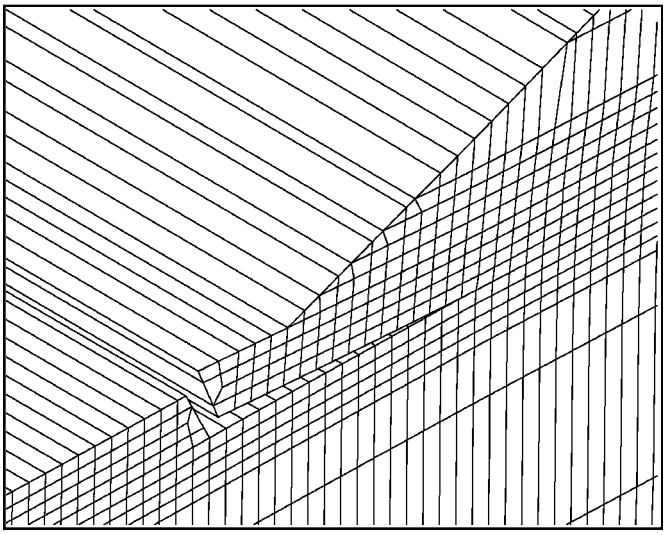

(c) Detail of deformed model of damaged specimen

FIGURE 5. *Full three-dimensional model of skin/flange specimen*

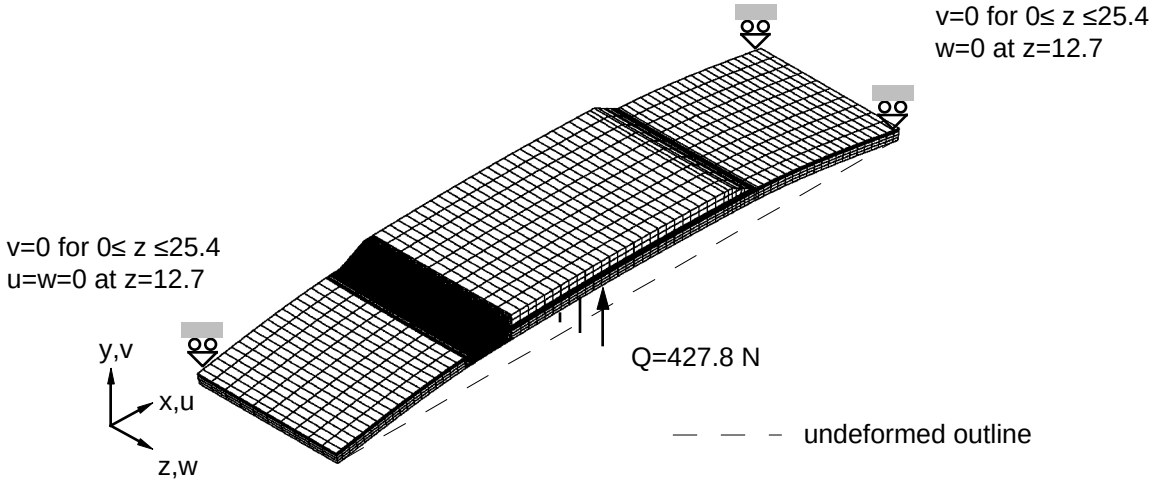

(a) Deformed three-dimensional model with load and boundary conditions

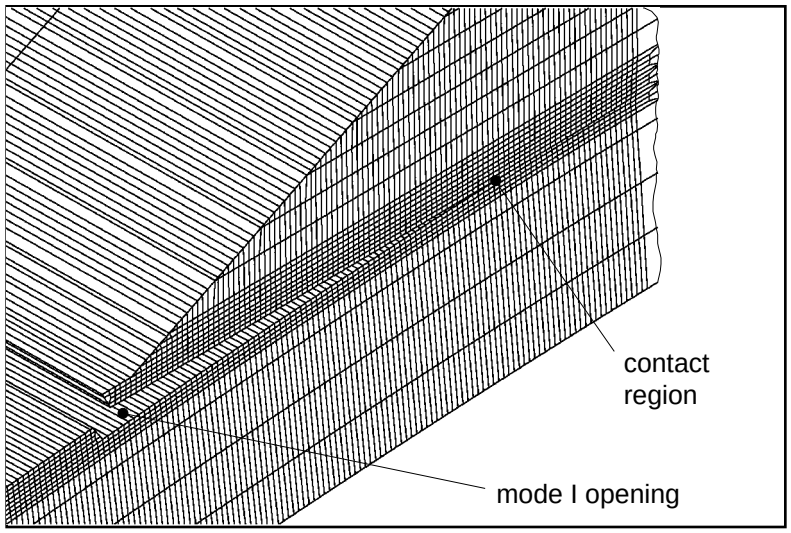

(b) Detail of deformed model of damaged specimen

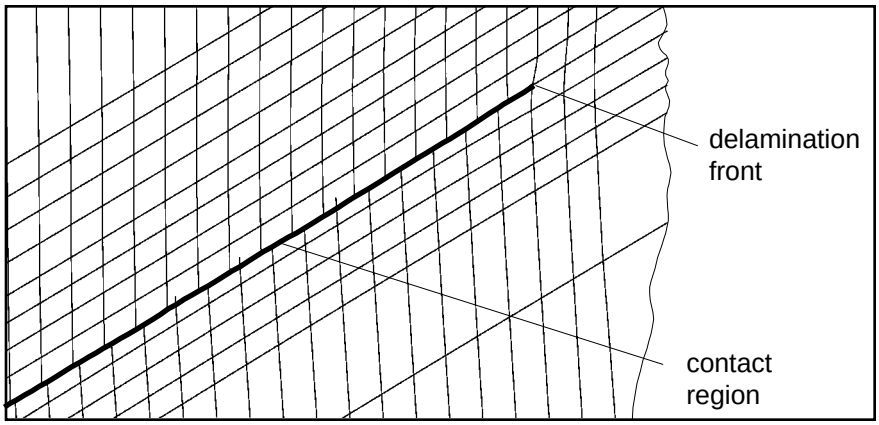

(c) Detail of contact region

FIGURE 6. *Full three-dimensional model of skin/flange specimen subjected to three-point bending*

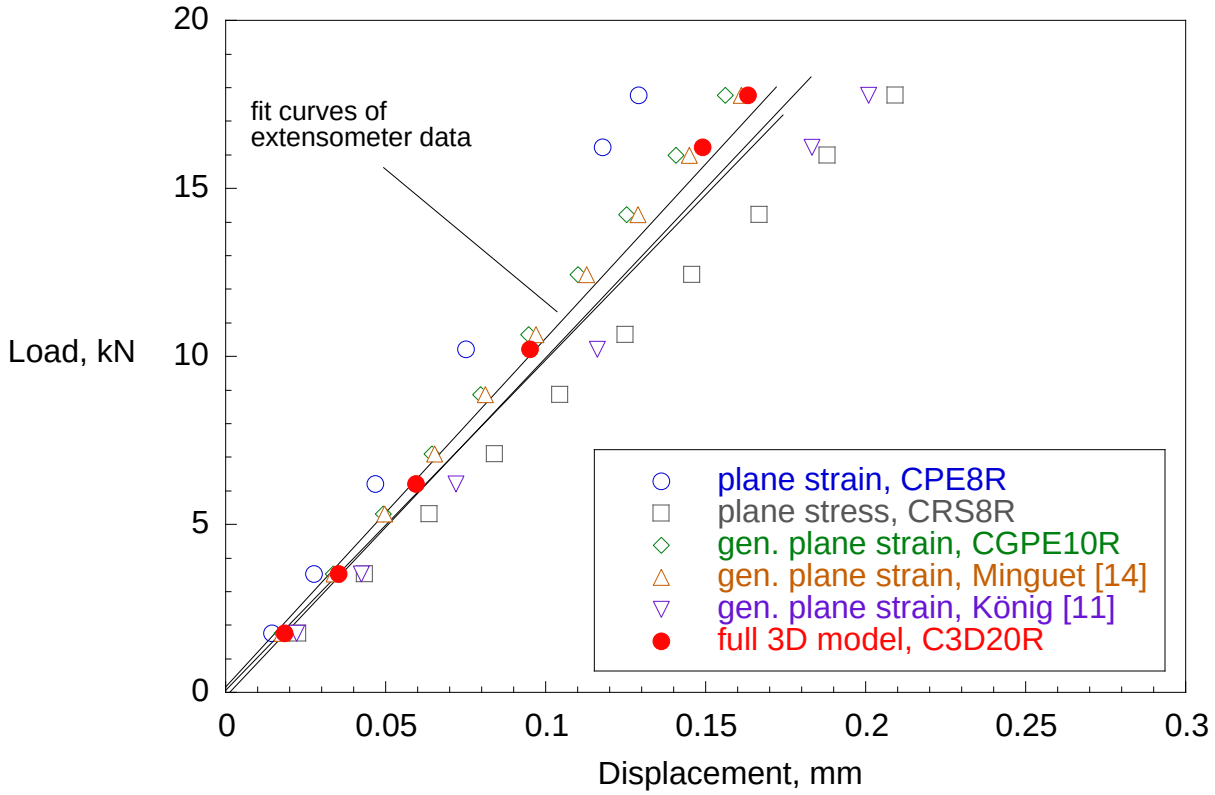

FIGURE 7. *Load-displacement plots for tension tests.*

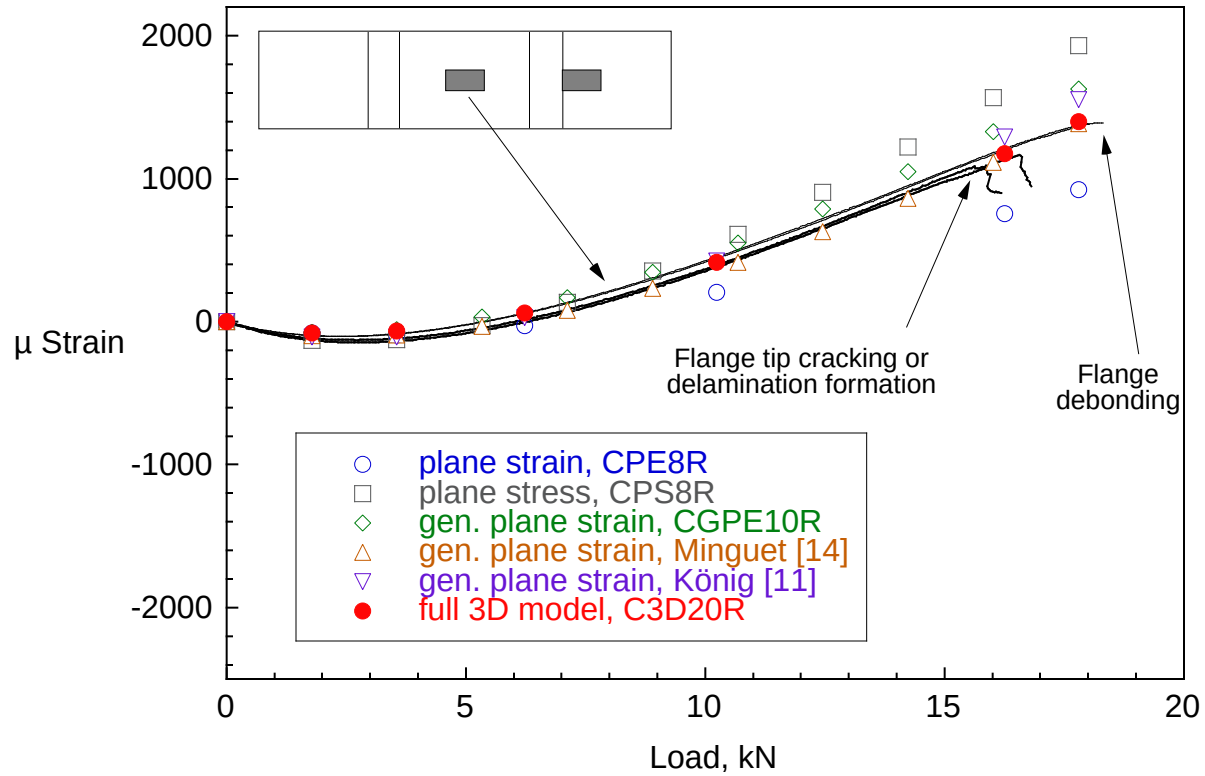

FIGURE 8. *Flange strain-load plots for tension tests*

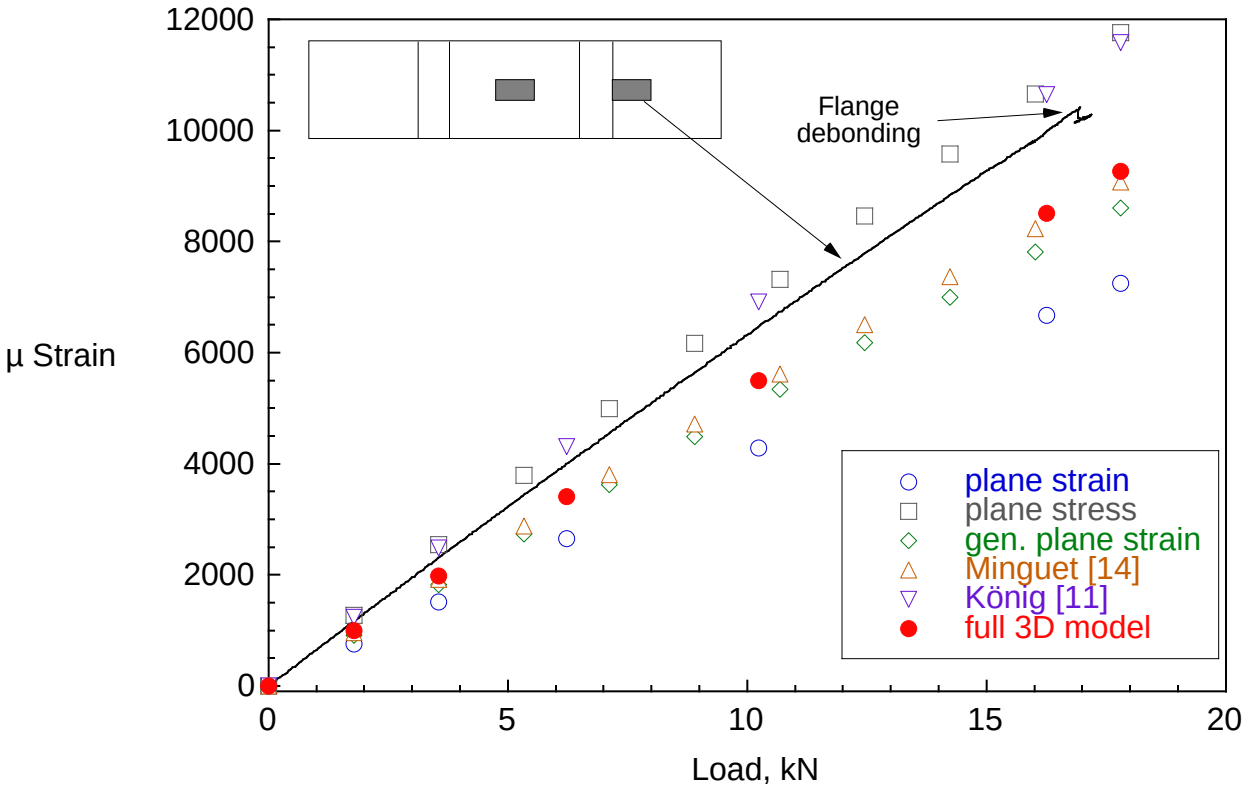

FIGURE 9. *Typical skin strain-load plot for tension tests.*

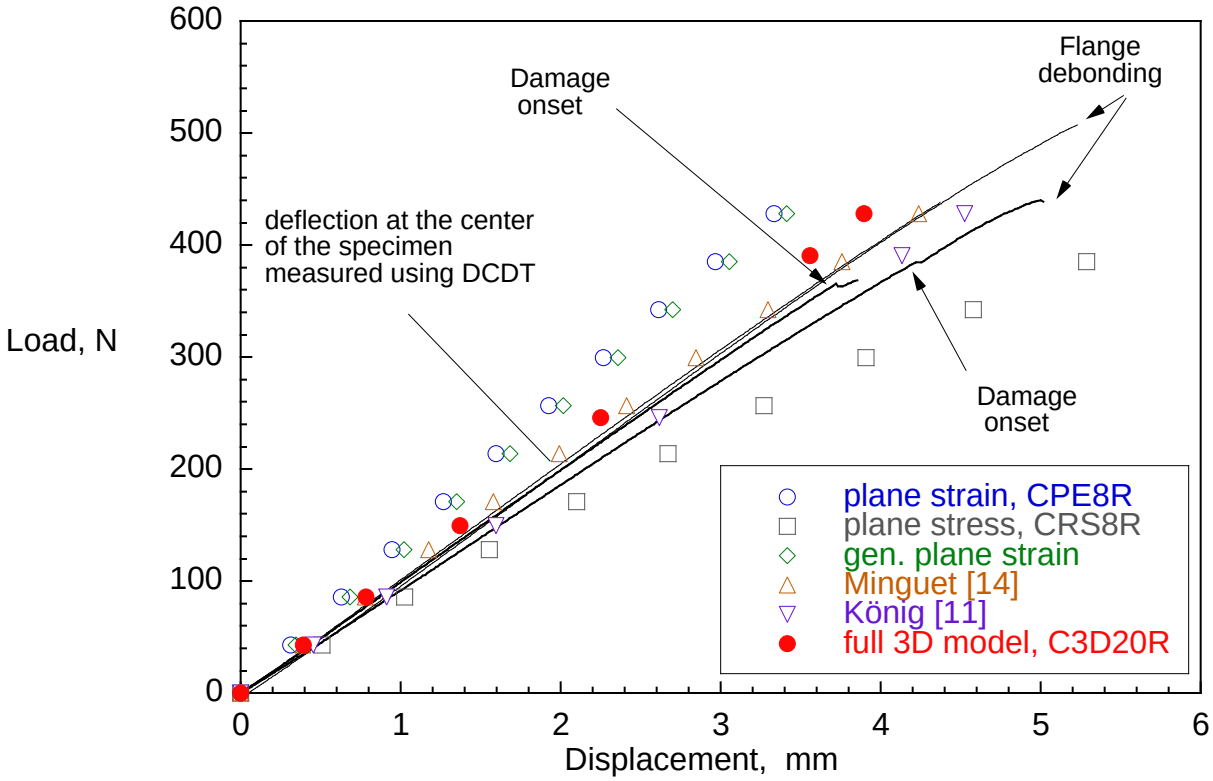

FIGURE 10. *Load-displacement plots for three-point bending tests*

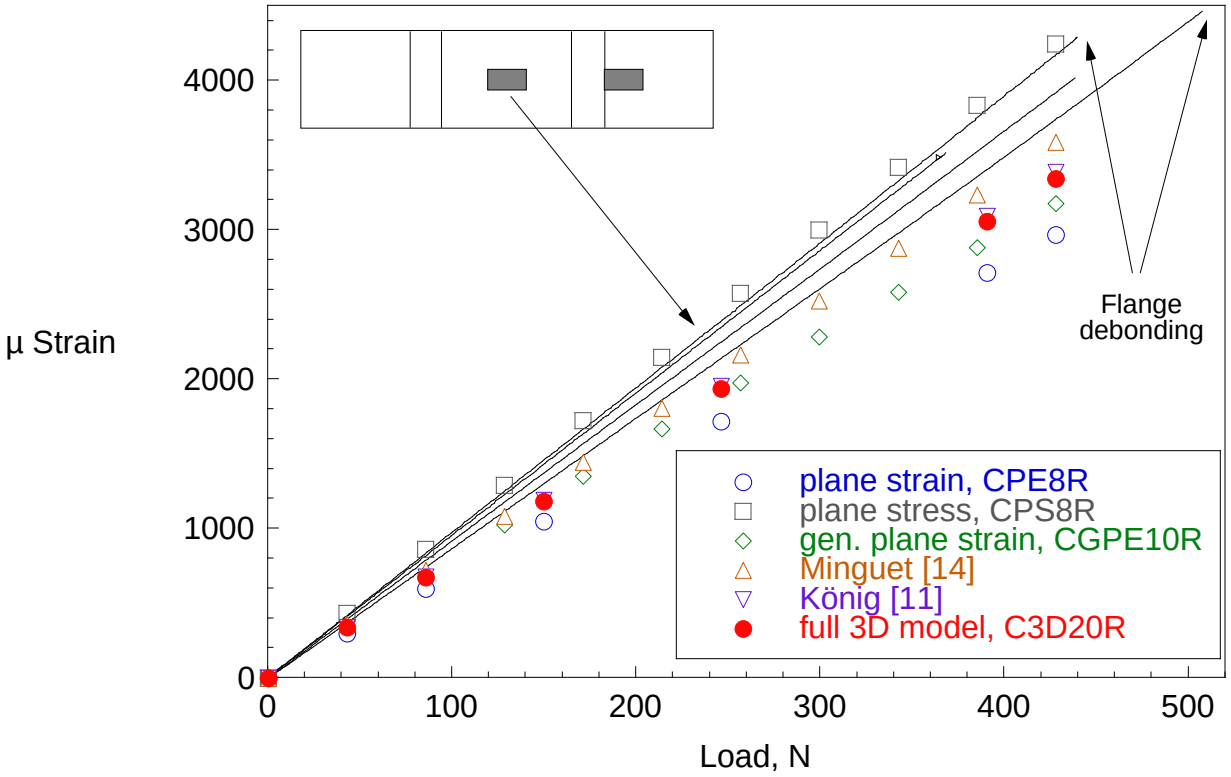

FIGURE 11. *Flange strain-load plot for three-point bending tests*

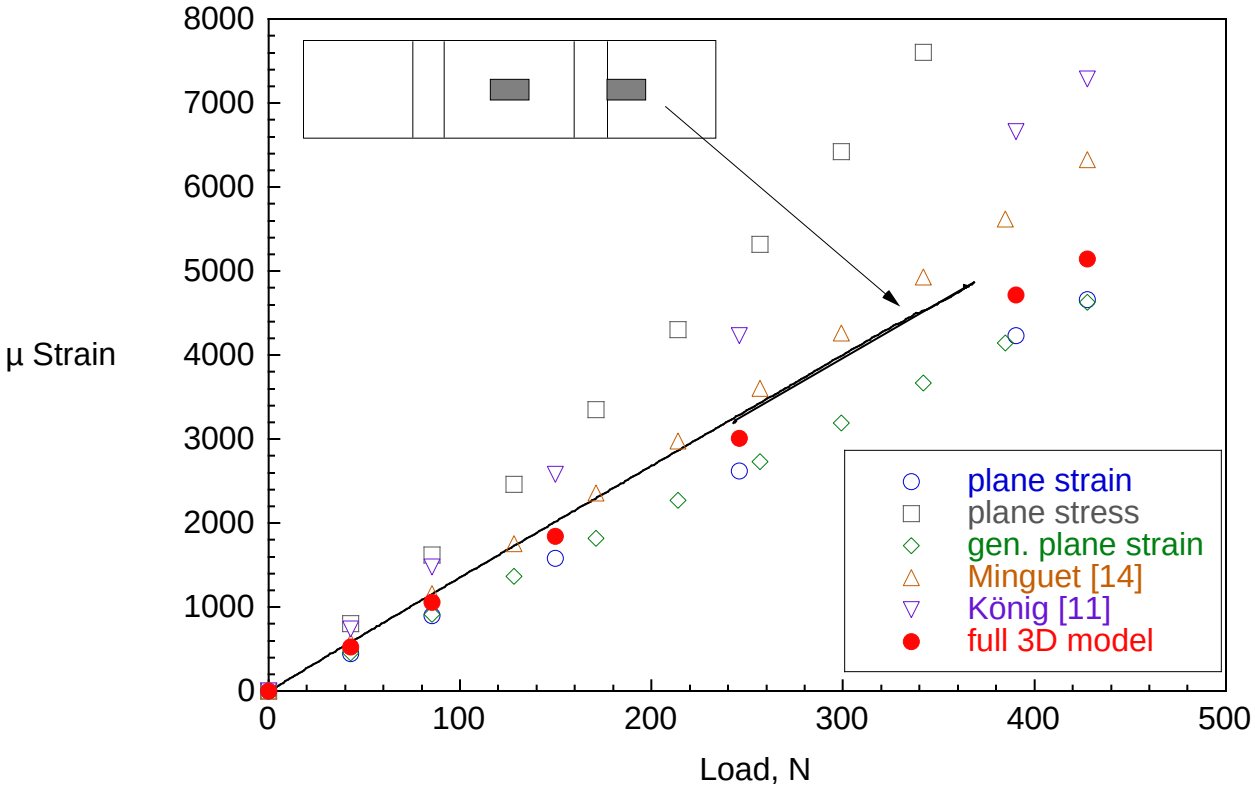

FIGURE 12. *Skin strain-load plot for three-point bending tests*

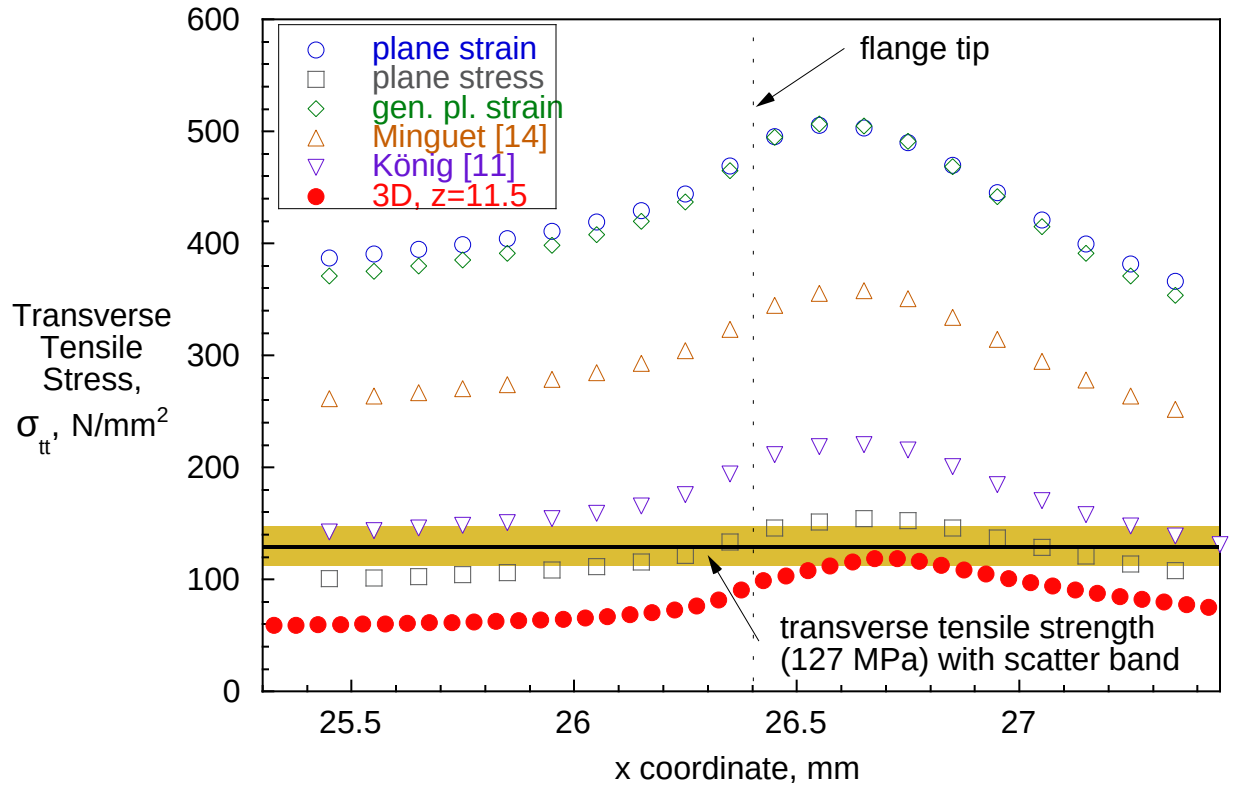

FIGURE 13. *Computed transverse tensile stress results in top 45° skin ply for tension test*

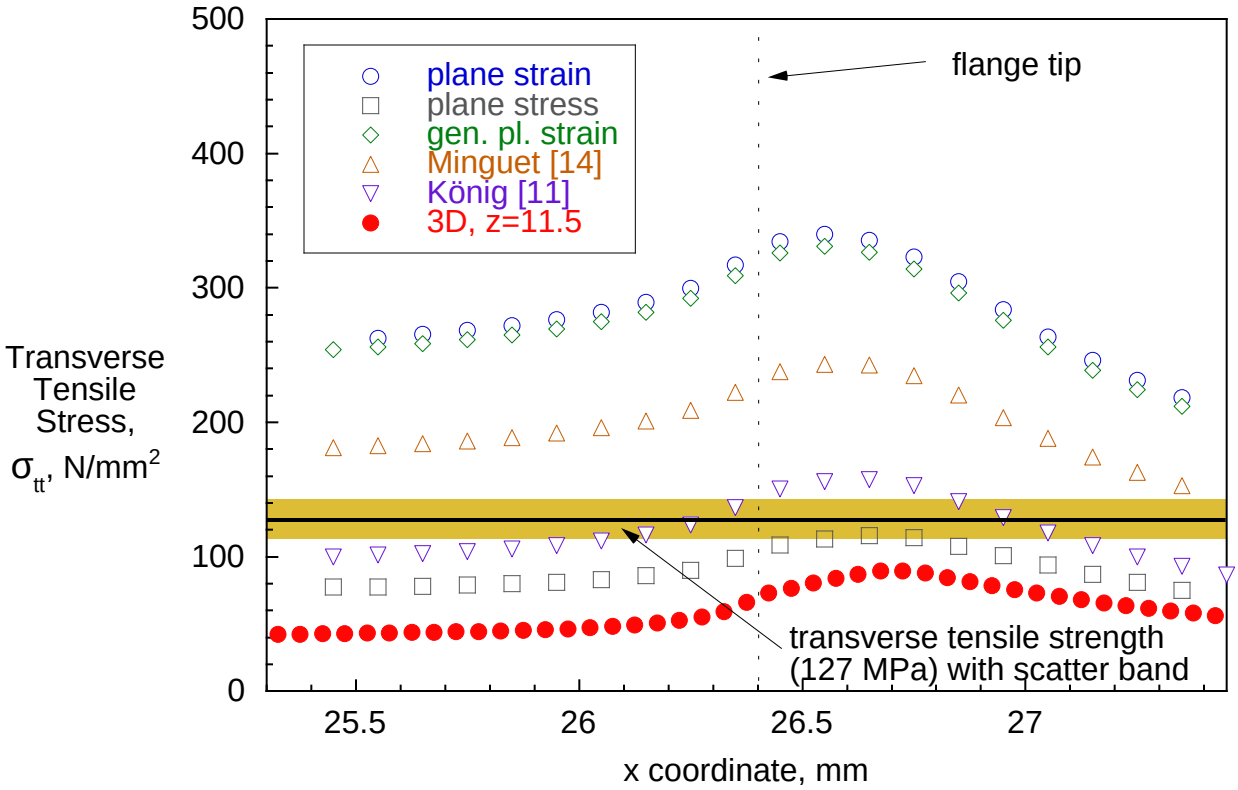

FIGURE 14. *Computed transverse tensile stress results in top 45° skin ply for three-point bending test*

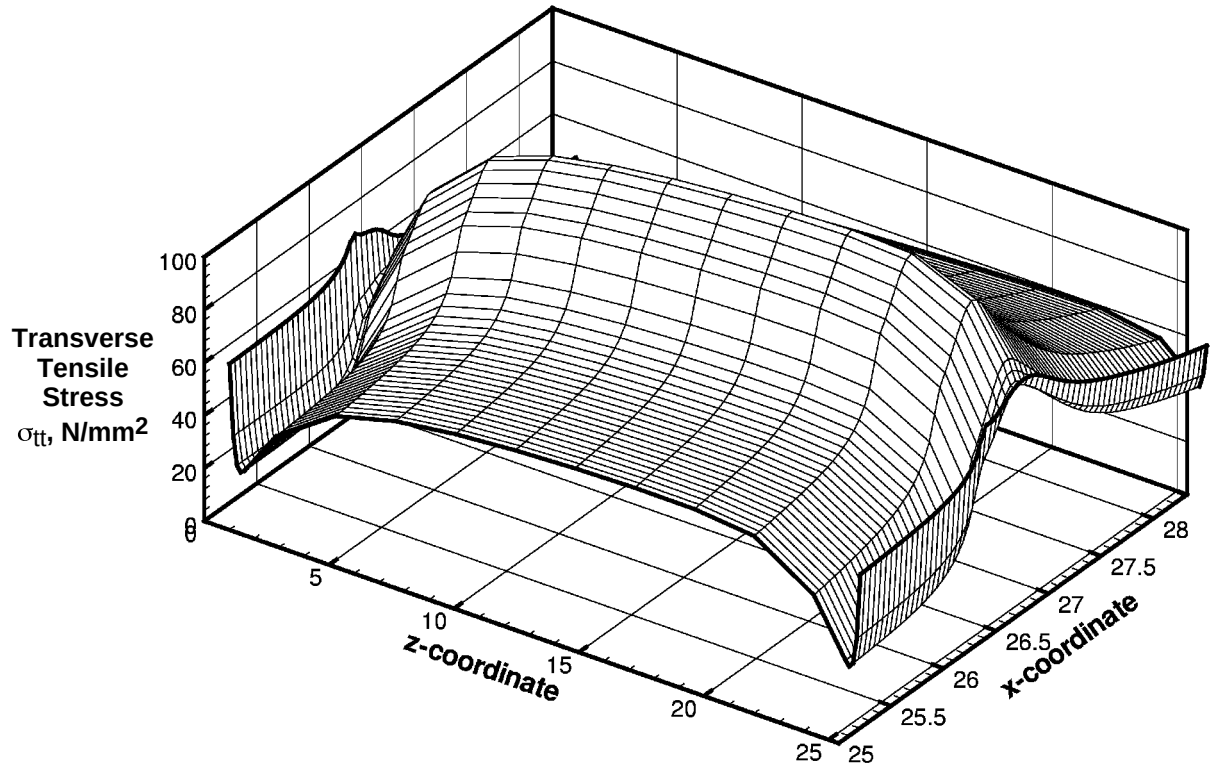

FIGURE 15. *Computed transverse tensile stress distribution in top 45° skin ply for tension test.*

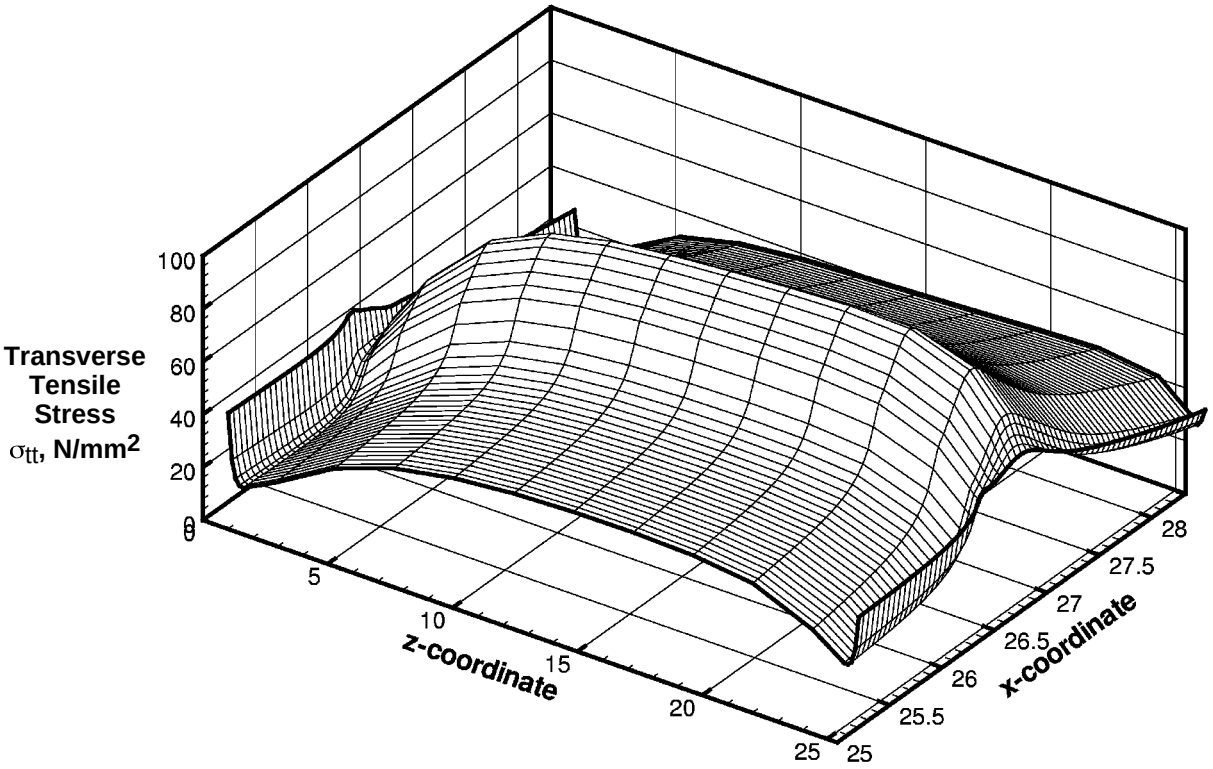

FIGURE 16. *Computed transverse tensile stress distribution in top 45° skin ply for three-point bending test.*

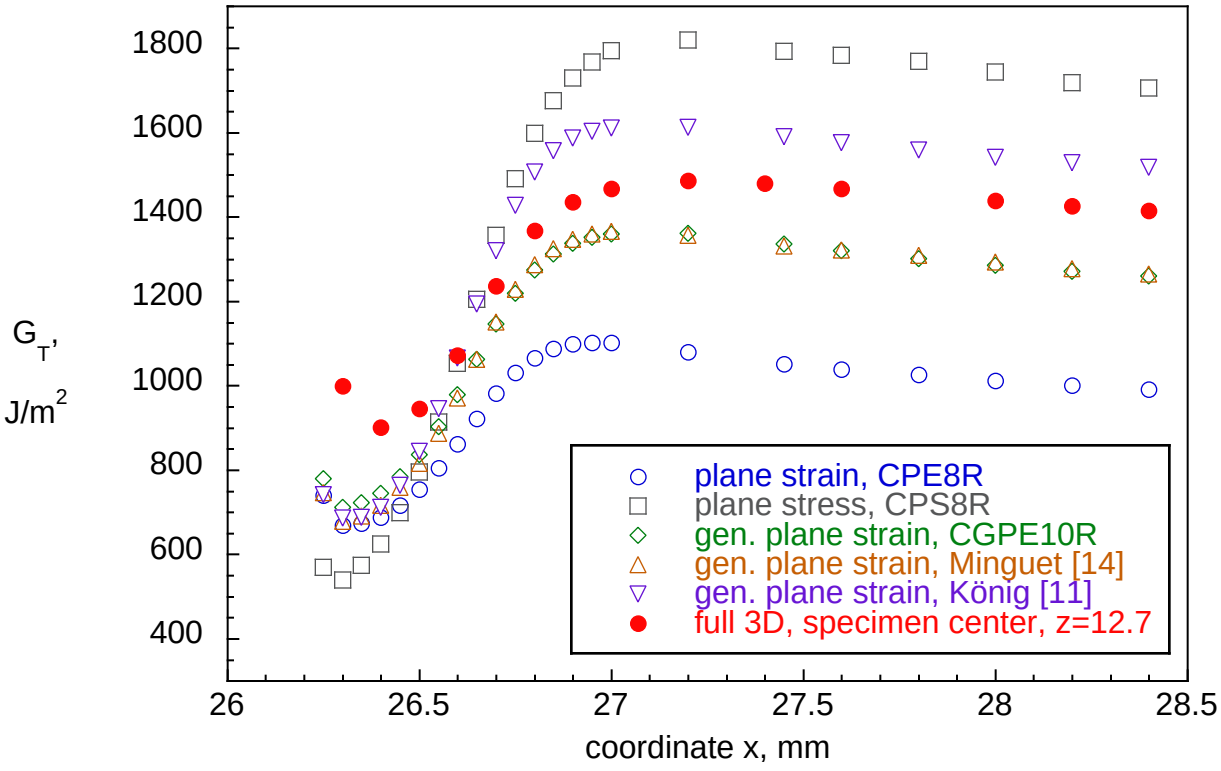

FIGURE 17. *Computed total energy release rate for delamination growing from matrix crack in skin top 45°/-45°ply interface for tension test*

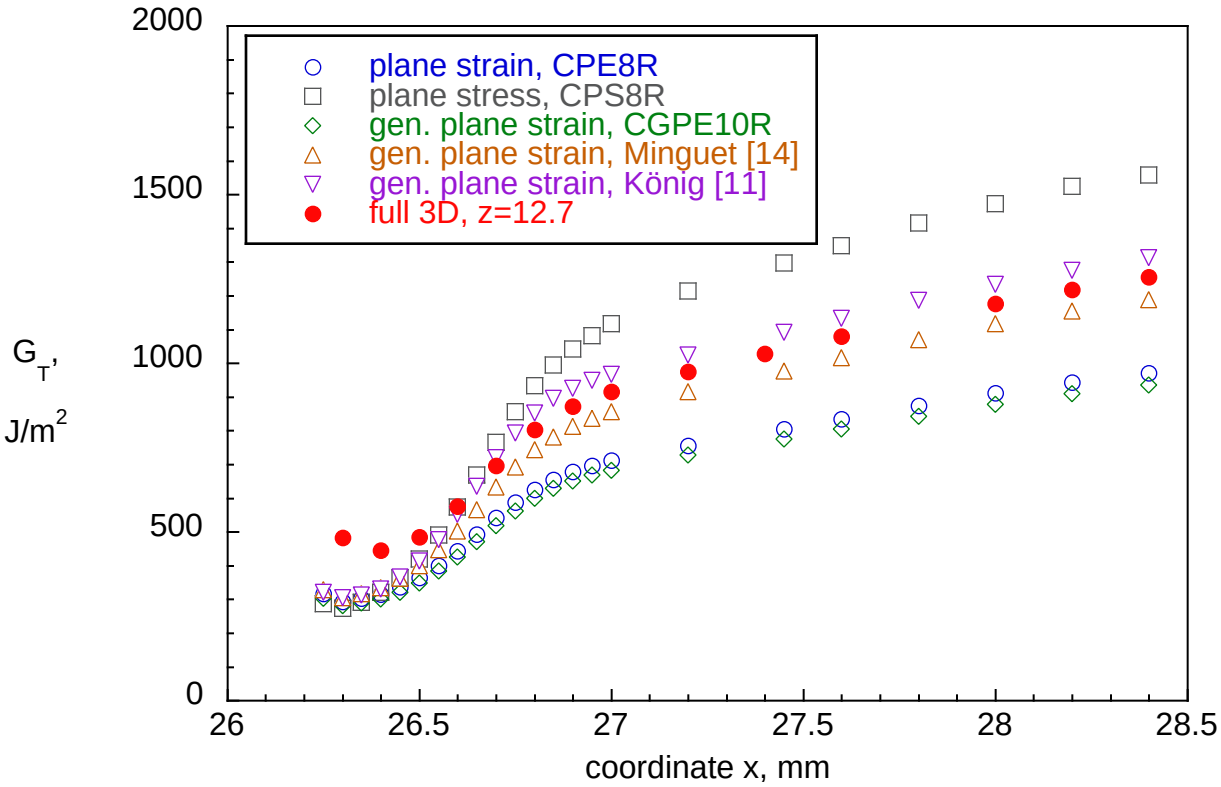

FIGURE 18. *Computed total energy release rate for delamination growing from matrix crack in skin top 45°/-45°ply interface for three-point bending test*

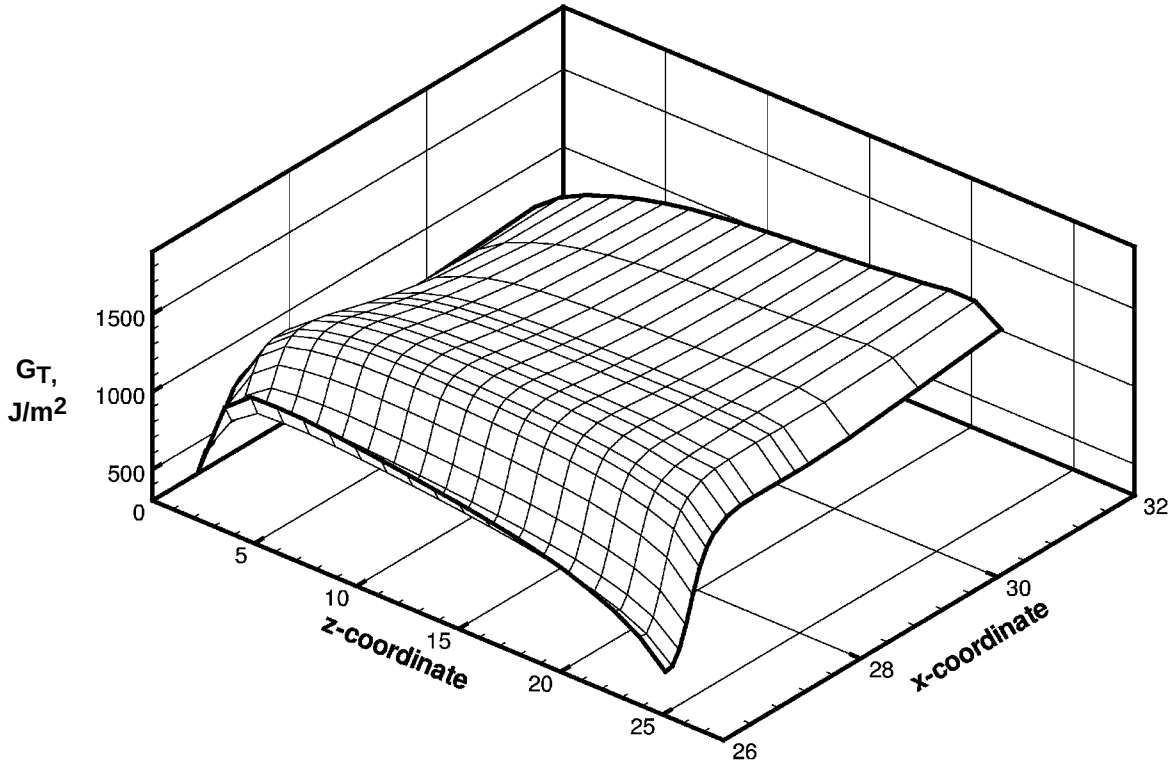

FIGURE 19. *Computed total energy release rate distribution for tension test.*

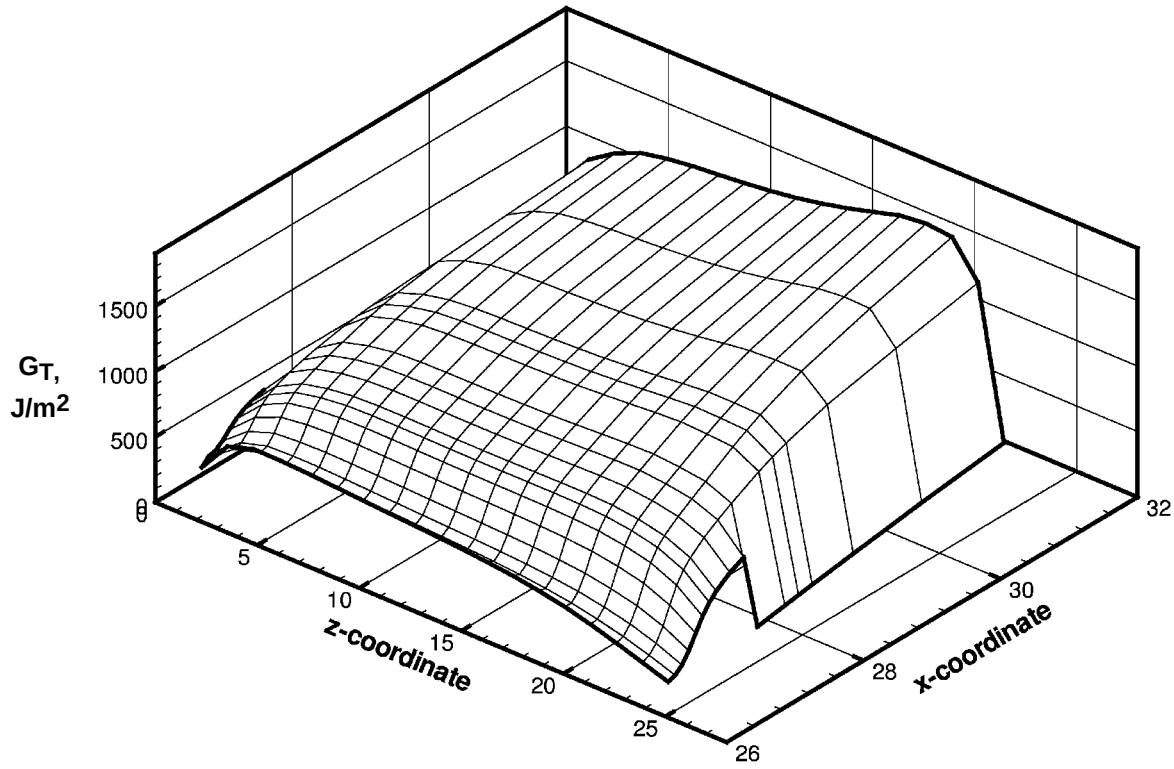

FIGURE 20. *Computed total energy release rate distribution for three-point bending test.*

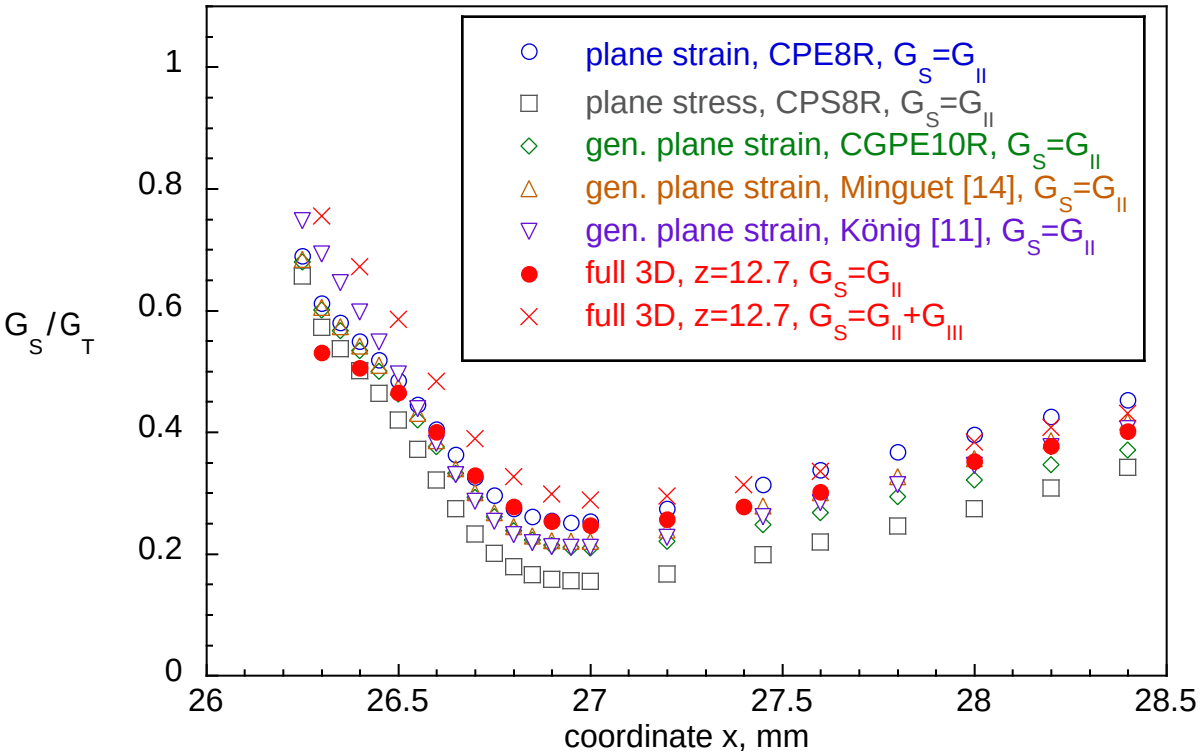

FIGURE 21. *Computed mixed mode ratio G_S/G_T for delamination growing from matrix crack in skin top 45°/-45°ply interface (tension test)*

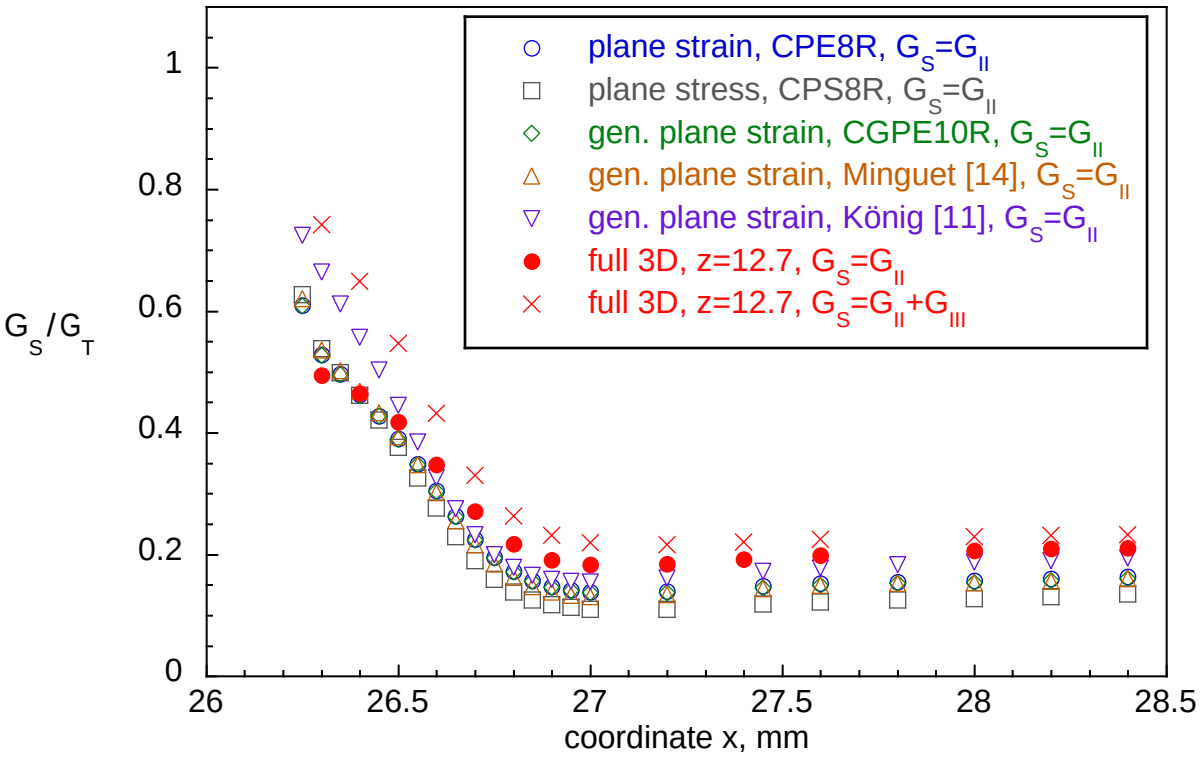

FIGURE 22. *Computed mixed mode ratio G_S/G_T for delamination growing from matrix crack in skin top 45°/-45°ply interface (three-point bending test)*

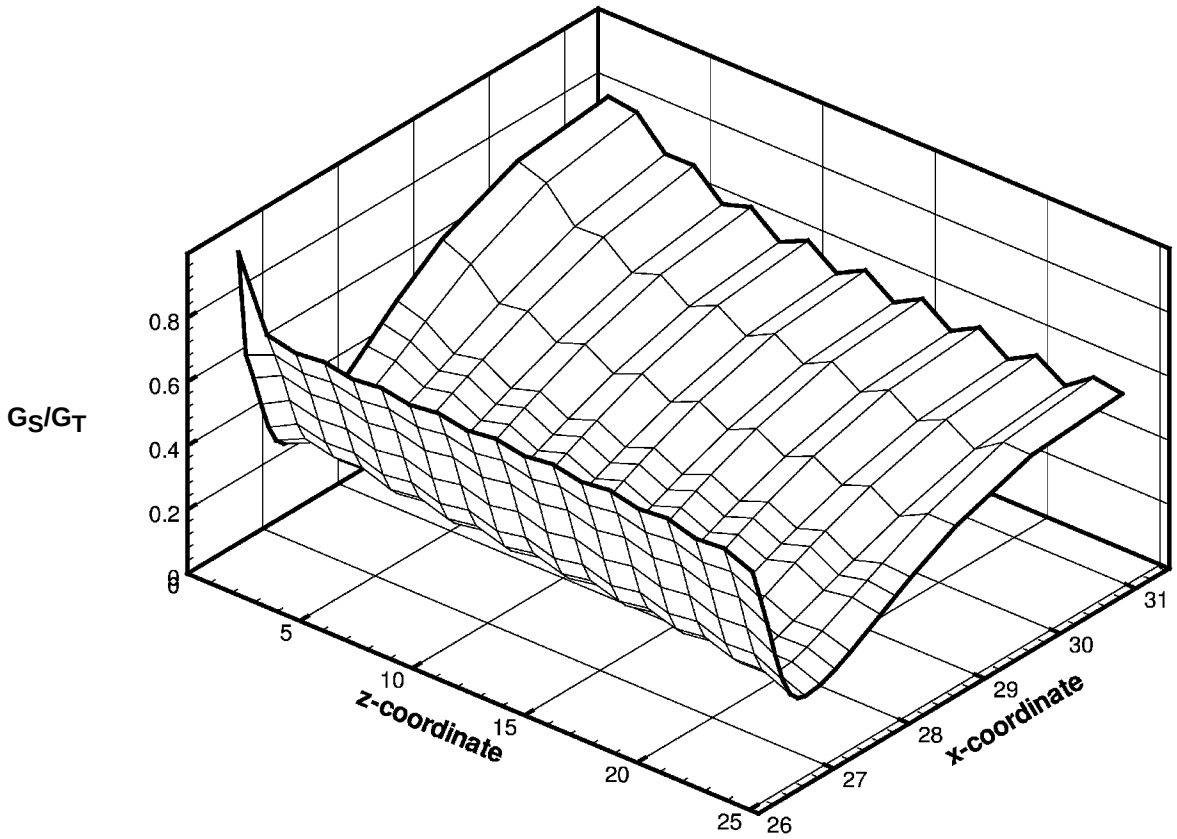

FIGURE 23. *Computed mixed mode ratio G_S/G_T for tension test.*

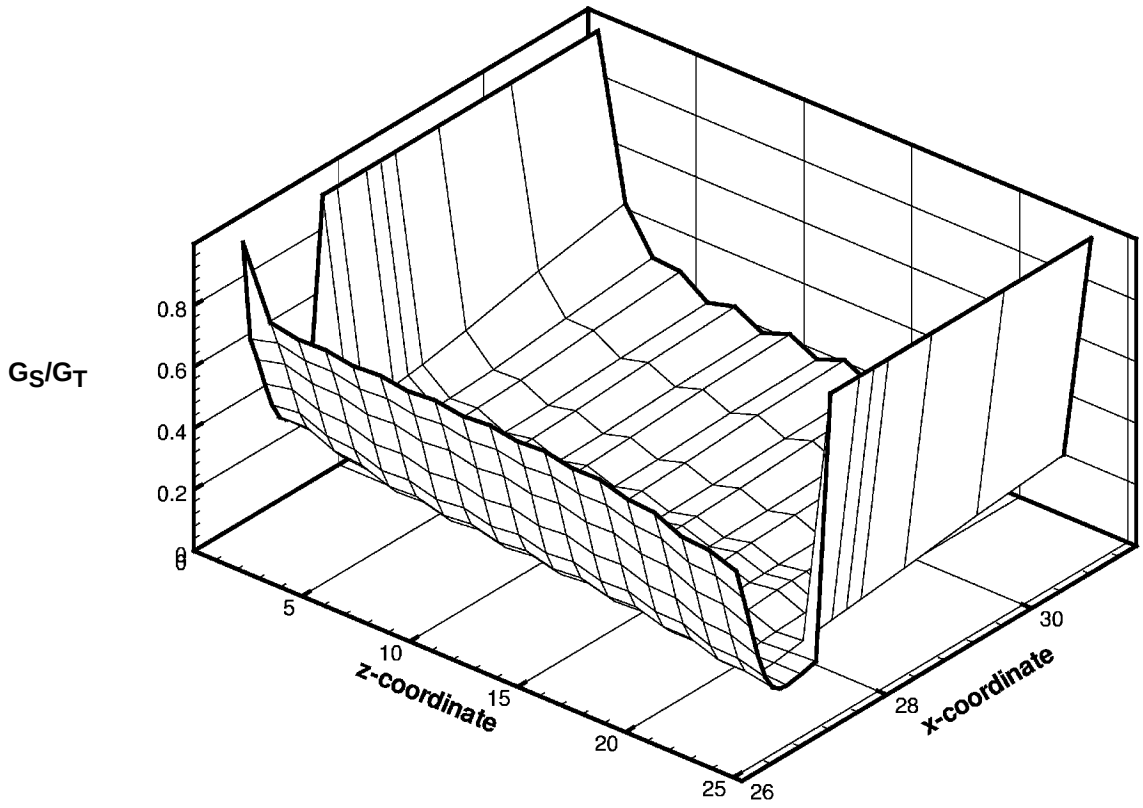

FIGURE 24. *Computed mixed mode ratio G_S/G_T for three-point bending tes*t.

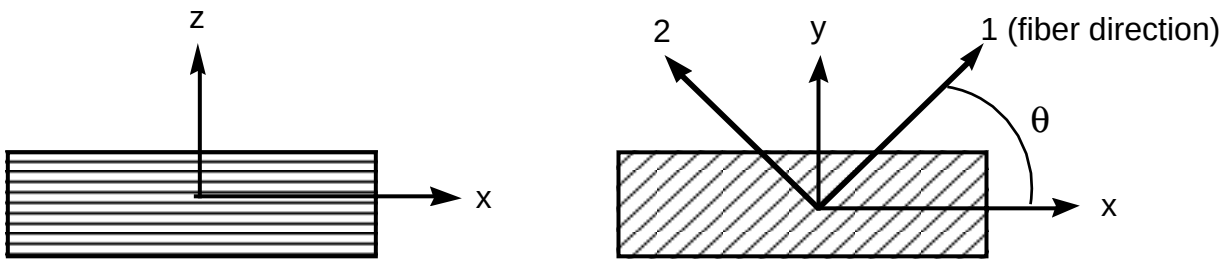

FIGURE A1. *Laminate coordinate system*

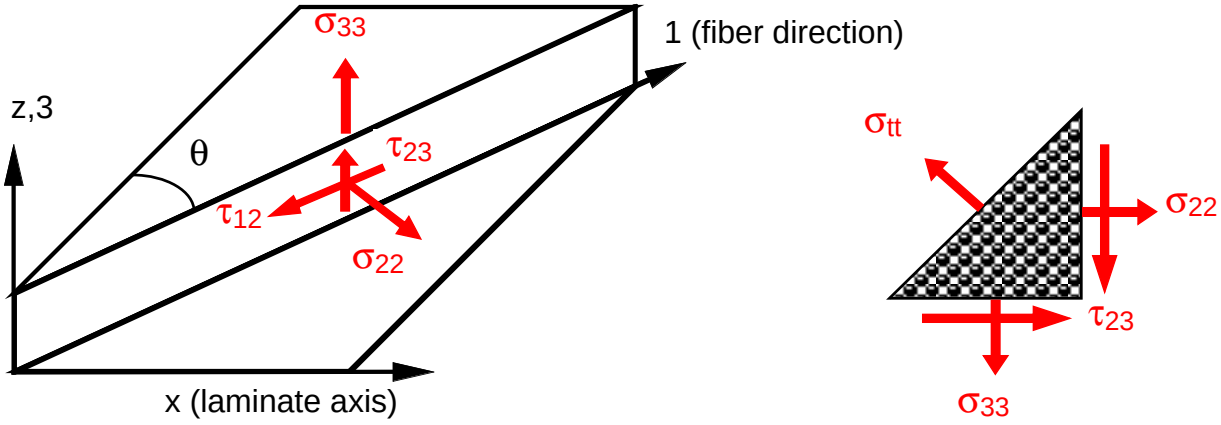

FIGURE A2. *Definition of ply transverse tensile stress.*

REPORT DOCUMENTATION PAGE

Form Approved
OMB No. 0704-0188

Public reporting burden for this collection of information is estimated to average 1 hour per response, including the time for reviewing instructions, searching existing data sources, gathering and maintaining the data needed, and completing and reviewing the collection of information. Send comments regarding this burden estimate or any other aspect of this collection of information, including suggestions for reducing this burden, to Washington Headquarters Services, Directorate for Information Operations and Reports, 1215 Jefferson Davis Highway, Suite 1204, Arlington, VA 22202-4302, and to the Office of Management and Budget, Paperwork Reduction Project (0704-0188), Washington, DC 20503.

1. AGENCY USE ONLY *(Leave blank)*	2. REPORT DATE	3. REPORT TYPE AND DATES COVERED
	March 2002	Contractor Report

4. TITLE AND SUBTITLE
Influence of 2D finite element modeling assumptions on debonding prediction for composite skin-stiffener specimens subjected to tension and bending

5. FUNDING NUMBERS
C NAS1-97046
WU 505-90-52-01

6. AUTHOR(S)
Ronald Krueger and Pierre J. Minguet

7. PERFORMING ORGANIZATION NAME(S) AND ADDRESS(ES)
ICASE
Mail Stop 132C
NASA Langley Research Center
Hampton, VA 23681-2199

8. PERFORMING ORGANIZATION REPORT NUMBER
ICASE Report No. 2002-4

9. SPONSORING/MONITORING AGENCY NAME(S) AND ADDRESS(ES)
National Aeronautics and Space Administration
Langley Research Center
Hampton, VA 23681-2199

10. SPONSORING/MONITORING AGENCY REPORT NUMBER
NASA/CR-2002-211452
ICASE Report No. 2002-4

11. SUPPLEMENTARY NOTES
Langley Technical Monitor: Dennis M. Bushnell
Final Report
To be presented at the International Conference on Composite Structures.

12a. DISTRIBUTION/AVAILABILITY STATEMENT
Unclassified–Unlimited
Subject Category 34
Distribution: Nonstandard
Availability: NASA-CASI (301) 621-0390

12b. DISTRIBUTION CODE

13. ABSTRACT *(Maximum 200 words)*
The influence of two-dimensional finite element modeling assumptions on the debonding prediction for skin-stiffener specimens was investigated. Geometrically nonlinear finite element analyses using two-dimensional plane-stress and plane-strain elements as well as three different generalized plane strain type approaches were performed. The computed deflections, skin and flange strains, transverse tensile stresses and energy release rates were compared to results obtained from three-dimensional simulations. The study showed that for strains and energy release rate computations the generalized plane strain assumptions yielded results closest to the full three-dimensional analysis. For computed transverse tensile stresses the plane stress assumption gave the best agreement. Based on this study it is recommended that results from plane stress and plane strain models be used as upper and lower bounds. The results from generalized plane strain models fall between the results obtained from plane stress and plane strain models. Two-dimensional models may also be used to qualitatively evaluate the stress distribution in a ply and the variation of energy release rates and mixed mode ratios with delamination length. For more accurate predictions, however, a three-dimensional analysis is required.

14. SUBJECT TERMS
composite materials, delamination, finite element analysis, fracture mechanics

15. NUMBER OF PAGES
35

16. PRICE CODE
A03

17. SECURITY CLASSIFICATION OF REPORT	18. SECURITY CLASSIFICATION OF THIS PAGE	19. SECURITY CLASSIFICATION OF ABSTRACT	20. LIMITATION OF ABSTRACT
Unclassified	Unclassified		